Ion channel-kinase TRPM7 is required for maintaining cardiac automaticity

Rajan Sah[a,b,c], Pietro Mesirca[d,e], Marjolein Van den Boogert[a], Jonathan Rosen[b], John Mably[b], Matteo E. Mangoni[d,e], and David E. Clapham[a,f,1]

[a]Howard Hughes Medical Institute, [b]Department of Cardiology, Boston Children's Hospital, Boston, MA 02115; [c]Cardiovascular Division, Brigham and Women's Hospital, Boston, MA 02115; [d]Universités de Montpellier 1 and 2, Centre National de la Recherche Scientifique, Unité Mixte de Recherche 5203, Institut de Génomique Fonctionnelle, Département de Physiologie, LabEx Ion Channels Science and Therapeutics, F-34094 Montpellier, France; [e]Institut National de la Santé et de la Recherche Médicale U661, F-34094 Montpellier, France; and [f]Department of Neurobiology, Harvard Medical School, Boston, MA 02115

Contributed by David E. Clapham, June 25, 2013 (sent for review May 26, 2013)

Sick sinus syndrome and atrioventricular block are common clinical problems, often necessitating permanent pacemaker placement, yet the pathophysiology of these conditions remains poorly understood. Here we show that *T*ransient *R*eceptor *P*otential *M*elastatin *7* (TRPM7), a divalent-permeant channel-kinase of unknown function, is highly expressed in embryonic myocardium and sinoatrial node (SAN) and is required for cardiac automaticity in these specialized tissues. TRPM7 disruption in vitro, in cultured embryonic cardiomyocytes, significantly reduces spontaneous Ca^{2+} transient firing rates and is associated with robust down-regulation of *Hcn4*, $Ca_v3.1$, and *SERCA2a* mRNA. TRPM7 knockdown in zebrafish, global murine cardiac *Trpm7* deletion ($KO^{\alpha MHC\text{-}Cre}$), and tamoxifen-inducible SAN restricted *Trpm7* deletion ($KO^{HCN4\text{-}CreERT2}$) disrupts cardiac automaticity in vivo. Telemetered and sedated $KO^{\alpha MHC\text{-}Cre}$ and $KO^{HCN4\text{-}CreERT2}$ mice show episodes of sinus pauses and atrioventricular block. Isolated SAN from $KO^{\alpha MHC\text{-}Cre}$ mice exhibit diminished Ca^{2+} transient firing rates with a blunted diastolic increase in Ca^{2+}. Action potential firing rates are diminished owing to slower diastolic depolarization. Accordingly, *Hcn4* mRNA and the pacemaker current, I_f, are diminished in SAN from both $KO^{\alpha MHC\text{-}Cre}$ and $KO^{HCN4\text{-}CreERT2}$ mice. Moreover, heart rates of $KO^{\alpha MHC\text{-}Cre}$ mice are less sensitive to the selective I_f blocker ivabradine, and acute application of the recently identified TRPM7 blocker FTY720 has no effect on action potential firing rates of wild-type SAN cells. We conclude that TRPM7 influences diastolic membrane depolarization and automaticity in SAN indirectly via regulation of *Hcn4* expression.

arrhythmia | electrocardiogram | electrophysiology | confocal

Sinus node dysfunction and atrioventricular node block (AVB) are common causes of bradyarrhythmias in patients, often requiring treatment with permanent pacemakers (1). However, the pathophysiology of sinus node failure and the physiology underlying sinoatrial node (SAN) automaticity remains incompletely understood. The currently held paradigm is that cardiac automaticity arises from the integrated activity of voltage-gated ionic currents (*Hcn2*/*Hcn4*, $Ca_v3.1$, $Ca_v1.3$), transporters (*NCX*), and sarcoplasmic reticulum (SR) Ca^{2+} release (2–4). In addition to these "classic" ion currents, some members of the transient receptor potential (TRP) superfamily of ion channels are also expressed in myocardium (TRPC1/3/4/6, TRPM4, TRPM7) (5, 6), but the contribution of these channels to myocardial function remains relatively unexplored.

Among these TRP channels, TRPM7 is especially abundant in both human and murine heart (5, 6) and is concentrated in myocardium during embryonic development (7). TRPM7, and its homolog TRPM6, are unique in that they are ion channels containing a carboxyl terminal kinase of unknown function. TRPM7 channel is divalent-permeant and forms an outwardly rectifying current that is inhibited by both cytoplasmic and extracellular Mg^{2+} (8). TRPM7 current was recently shown to be up-regulated in human atrial fibroblasts in the context of atrial fibrillation and was hypothesized to provide a Ca^{2+} influx pathway inducing TGF-β1–mediated fibroblast proliferation and differentiation, thereby contributing to atrial fibrosis in the pathogenesis of atrial fibrillation (9). In addition to atrial fibroblasts, ventricular fibroblasts also have a large TRPM7 current (10), and a TRPM7-like current has been recorded from human atrial myocytes (11). Thus, TRPM7 represents a heretofore unstudied ionic current and signaling molecule in cardiac biology that may participate in arrhythmogenesis in human heart disease or contribute to normal myocardial Ca^{2+} signaling.

In this study we show that TRPM7 is required for maintaining cardiac automaticity. TRPM7 current is largest in myocardial cells that exhibit automaticity, such as cultured embryonic ventricular cardiomyocytes (EVM) and isolated SAN cells, compared with the quiescent adult ventricular cardiomyocyte (AVM). *Trpm7* deletion in both EVM and SAN slows spontaneous Ca^{2+} transient frequency, thereby disrupting cardiac automaticity in vitro. In vivo, *Trpm7* loss of function slows heart rate in embryonic zebrafish and induces sinus pauses (SPs) and AVB in both global cardiac-targeted *Trpm7* knockout mice ($KO^{\alpha MHC\text{-}Cre}$) and in tamoxifen-inducible SAN/atrioventricular node cell (AVN)-restricted *Trpm7* knockout mice ($KO^{Hcn4\text{-}CreERT2}$). We show that these effects are associated with shallowing of the diastolic depolarization slope (DDSL) due to TRPM7-dependent down-regulation of *Hcn4* and pacemaker current, I_f.

Results

***Trpm7* Deletion in Vitro Disrupts Cardiac Automaticity in Cultured Murine Embryonic Cardiomyocytes.** We previously showed that TRPM7 is predominantly expressed in the heart of embryonic

Significance

***T*ransient *R*eceptor *P*otential *M*elastatin *7* (TRPM7) is a divalent-permeant channel-kinase of unknown function expressed in human atrial myocytes and fibroblasts and recently implicated in atrial arrhythmias. We show that TRPM7 is highly expressed in embryonic myocardium and sinoatrial node (SAN). *Trpm7* disruption in vitro, in cultured embryonic cardiomyocytes, and in vivo in zebrafish and in mice impairs cardiac automaticity. We show that this occurs via reductions in *Hcn4* mRNA and the pacemaker current, I_f, in SAN. We conclude that TRPM7 influences diastolic membrane depolarization and automaticity in SAN via regulation of *Hcn4* expression.**

Author contributions: R.S. and D.E.C. designed research; R.S., P.M., M.V.d.B., and J.R. performed research; R.S. and J.M. contributed new reagents/analytic tools; R.S., P.M., and M.E.M. analyzed data; and R.S. and D.E.C. wrote the paper.

The authors declare no conflict of interest.

[1]To whom correspondence should be addressed. E-mail: dclapham@enders.tch.harvard.edu.

This article contains supporting information online at www.pnas.org/lookup/suppl/doi:10.1073/pnas.1311865110/-/DCSupplemental.

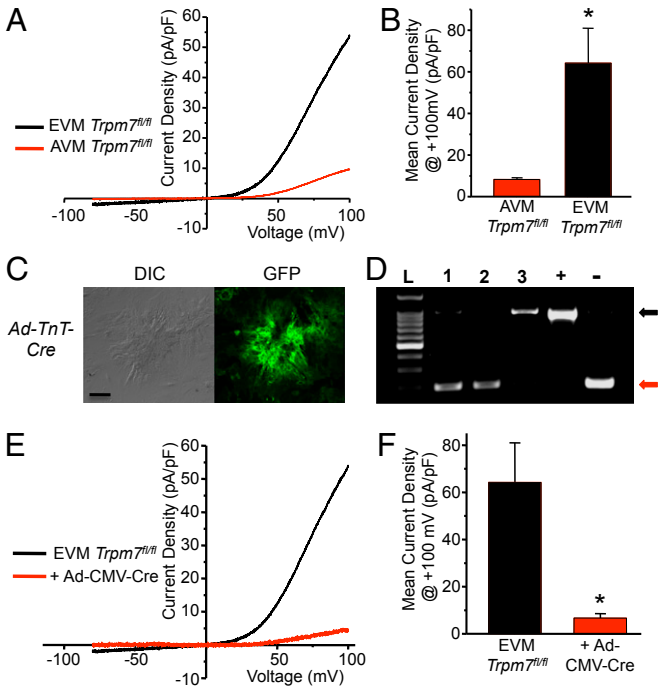

Fig. 1. TRPM7 current in cultured murine embryonic ventricular myocytes. (*A*) Representative TRPM7 current measured in cultured EVM compared with AVM after full run-up. (*B*) Mean TRPM7 current density at +100 mV in AVM ($I_{Trpm7,\ AVM}$ = 8.3 ± 0.9 pA/pF, n = 5) compared with EVM ($I_{Trpm7,\ EVM}$ = 64.2 ± 16.7 pA/pF, n = 5). (*C*) Interference contrast (DIC, *Left*) and fluorescence GFP image (*Right*). (*D*) PCR across exon 17 from genomic DNA isolated from $Trpm7^{fl/fl}$ EVM transduced with *Ad-TnT-Cre* (1), *Ad-CMV-Cre* (2), and *Ad-CMV-Lacz* (3), $Trpm7^{fl/fl}$ fibroblasts (+), and $Trpm7^{fl/-}$ tail (-). Black arrow, full-length exon 17. Red arrow, deleted exon 17. (*E*) Representative *TRPM7* current measured in $Trpm7^{fl/fl}$ EVM and $Trpm7^{fl/fl}$ EVM 5 d after transduction with *Ad-CMV-Cre*. (*F*) Mean TRPM7 current density in $Trpm7^{fl/fl}$ EVM treated with *Ad-CMV-Cre* (n = 3) compared with untreated $Trpm7^{fl/fl}$ EVM (n = 5). *P < 0.05.

day (E)9.5 embryos (7) and becomes ubiquitously expressed in later embryonic development (7) and into adulthood (5, 6). Because TRPM7 is first expressed in the developing embryonic heart (7), we examined TRPM7 current in cultured EVM isolated from E13.5–14 $Trpm7^{fl/fl}$ (7) embryos and compared these with TRPM7 current in freshly dissociated AVM. A large TRPM7-like current is activated in EVM ($I_{Trpm7,EVM}$ = 64.2 ± 16.7 pA/pF at +100 mV, n = 5), ~eightfold larger than AVM ($I_{Trpm7,AVM}$ = 8.3 ± 0.9 pA/pF, n = 5, P < 0.05; Fig. 1 *A* and *B*) under whole-cell conditions. These TRPM7-like currents are initially absent on "break-in" but then run up over the course of 10 min of cell dialysis to a steady-state level (Fig. S1). To confirm that these TRPM7-like currents are indeed TRPM7, we used Cre-loxP technology to genetically ablate *Trpm7* in murine EVM. The conditional *Trpm7* allele contained *loxP* sites flanking exon 17, and *Cre*-mediated recombination induces a frame shift that prevents expression of the ion channel and kinase domains of TRPM7 (7). We introduced Cre to cultured $Trpm7^{fl/fl}$ EVM using adenoviruses (*Ad*) that drive Cre expression under either cytomegalovirus (*CMV*: ubiquitous) or troponin-T (*TnT*: cardiac-specific) promoters (*Ad-CMV-Cre*/*Ad-TnT-Cre*). An adenovirus expressing β-galactosidase (*Ad-CMV-Lacz*) served as a control. Using EVM isolated from E14 $ROSA26^{mTmG}$ embryos, we confirmed high-efficiency *Cre* transduction in EVM (>95%) by both *Ad-CMV-Cre* and *Ad-TnT-Cre* (Fig. 1*C*, only *Ad-TnT-Cre* shown). Genetic ablation of *Trpm7* exon 17 in $Trpm7^{fl/fl}$ EVM is evident by PCR within 2 d after adenoviral transduction with both *Ad-TnT-Cre* (Fig. 1*D*, lane 1) and *Ad-CMV-Cre* (lane 2) but not with *Ad-CMV-Lacz* (lane 3), according to the presence of the expected size of the deletion product in EVM genomic DNA. Finally, TRPM7 current is largely abolished in $Trpm7^{fl/fl}$ EVM treated with *Ad-CMV-Cre* when patch-clamped 4–5 d after adenoviral transduction (Fig. 1 *E* and *F*).

After 4 d in culture, *Ad-CMV-Lacz*–treated $Trpm7^{fl/fl}$ EVMs contract rhythmically at a significantly higher rate than either *Ad-CMV-Cre*- or *Ad-TnT-Cre*–treated EVM. To quantify this difference, we loaded EVM with Fluo-4AM and measured intracellular Ca^{2+} transients in clusters of *Ad-CMV-Lacz*-, *Ad-CMV-Cre*-, and *Ad-TnT-Cre*–treated $Trpm7^{fl/fl}$ EVM using high-speed laser scanning confocal microscopy (Fig. 2*A*). Ca^{2+} transient firing frequency is reduced equivalently ~twofold in EVM upon deletion of *Trpm7* by *Ad-CMV-Cre* (102 ± 18/min, n = 18, P < 0.01) and *Ad-TnT-Cre* (103 ± 17/min, n = 13, P < 0.01) compared with *Ad-CMV-Lacz* controls (206 ± 23/min, n = 18; Fig. 2*B*). Accordingly, cycle length increased ~twofold after *Trpm7* deletion (Fig. 2*C*). To control for possible off-target effects of Cre expression, we also compared cycle lengths of $Trpm7^{fl/+}$ EVM treated with *Ad-CMV-Cre* and *Ad-TnT-Cre* (Fig. S2). We find these no different from the *Ad-CMV-Lacz* controls. There is a small but statistically significant increase in peak Ca^{2+}

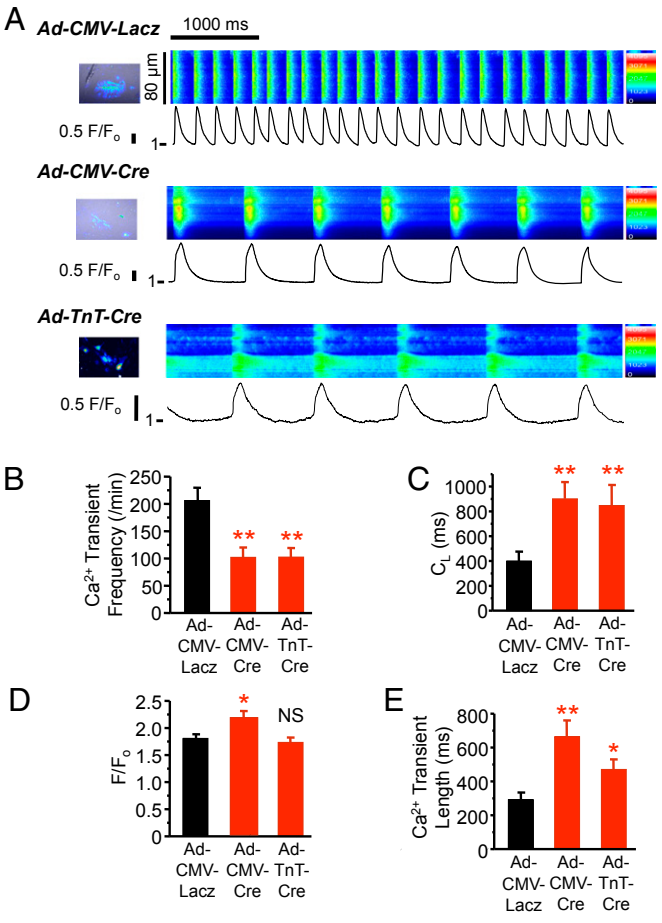

Fig. 2. *Trpm7* deletion in embryonic myocardium disrupts cardiac automaticity in vitro. (*A*) Ca^{2+} transients measured by high-speed line-scanning confocal microscopy in $Trpm7^{fl/fl}$ EVM 4–5 d after transduction with *Ad-CMV-Lacz* (*Top*), *Ad-CMV-Cre* (*Middle*), and *Ad-TnT-Cre* (*Bottom*). (*B*) Mean Ca^{2+} transient frequency, (*C*) cycle length, C_L, (*D*) peak Ca^{2+} transients, F/F_o, and (*E*) Ca^{2+} transient length in *Ad-CMV-Lacz*, *Ad-CMV-Cre*, and *Ad-TnT-Cre* treated $Trpm7^{fl/fl}$ EVMs. *P < 0.05, **P < 0.01.

transient amplitude upon *Trpm7* deletion with *Ad-CMV-Cre* ($F/F_{o\text{-CMV-Cre}} = 2.2 \pm 0.1$, $n = 19$, $P < 0.05$), but this is not observed in *Ad-TnT-Cre* ($F/F_{o\text{-TnT-Cre}} = 1.7 \pm 0.1$, $n = 12$) treated $Trpm7^{fl/fl}$ EVM compared with *Ad-CMV-Lacz* controls ($F/F_{o\text{-CMV-Lacz}} = 1.8 \pm 0.1$, $n = 19$; Fig. 2*D*). Additionally, Ca^{2+} transient duration is significantly lengthened in *Trpm7*-deleted EVM by both *Ad-CMV-Cre* (664 ± 96 ms, $n = 20$, $P < 0.01$) and *Ad-TnT-Cre* (471 ± 59 ms, $n = 12$, $P < 0.05$) compared with *Ad-CMV-Lacz* (291 ± 43, $n = 19$; Fig. 2*E*). Thus, TRPM7 deletion seems to slow spontaneous contractions and Ca^{2+} transient firing, in a cell autonomous fashion in cultured embryonic cardiomyocytes.

***Trpm7* Loss of Function in Vivo Disrupts Automaticity in Zebrafish and Induces Sinus Pauses and AVB in Mouse.** We next examined whether this effect of TRPM7 knockout on embryonic cardiac automaticity is also present in vivo in embryonic zebrafish. We find that the *Trpm7* morpholino (MO) zebrafish recapitulate the previously described phenotype of melanocyte deficiency and loss of touch responsiveness (12, 13) compared with water-injected controls. In addition, heart rates are ~25% lower in *Trpm7* MO zebrafish ($HR_{\text{Trpm7 MO}} = 80 \pm 2$ bpm, $n = 30$ embryos, $P < 0.001$) vs. controls ($HR_{\text{H20}} = 107 \pm 2$ bpm, $n = 27$ embryos; Fig. 3*A*), suggesting that the negative chronotropic effect of *TRPM7* disruption is not restricted to cultured murine EVM but also occurs in intact zebrafish embryos.

To determine whether TRPM7 is also important for automaticity in the adult mouse heart we turned to global cardiac TRPM7 knockout mice generated by crossing α*MHC-Cre* mice with $Trpm7^{fl/fl}$ and/or $Trpm7^{fl/-}$ mice ($KO^{\alpha MHC\text{-}Cre}$). Conscious electrocardiograms recorded over a 24-h period in freely moving telemetered $KO^{\alpha MHC\text{-}Cre}$ mice reveal frequent SPs (Fig. 3 *C* and *E* and Fig. S3 *B* and *F*) and AVB (Fig. 3 *D* and *F* and Fig. S3*D*) compared with no SP or AVB in *WT* mice (Fig. 3*B* and Fig. S3 *A* and *E*). $KO^{\alpha MHC\text{-}Cre}$ mice also exhibit SP with atrial bigeminy (Fig. S3 *C* and *F*) and ectopic atrial foci (Fig. S3 *B* and *G*) in both conscious, telemetered mice as well as in sedated mice. Despite the presence of these bradyarrhythmias in $KO^{\alpha MHC\text{-}Cre}$ mice, the mean heart rates over a 24-h period are not statistically different from *WT* (Fig. 3*G*).

TRPM7 Is Highly Expressed in Murine Sinoatrial Nodal Cells and Is Required for Normal SAN Automaticity. The SPs and AVB observed in $KO^{\alpha MHC\text{-}Cre}$ mice suggest that *Trpm7* deletion affects SAN and AVN function, because these are the specialized myocardial cell types that exhibit automaticity in the adult heart. To determine whether this was due to a direct effect of TRPM7 activity in SAN, we next examined TRPM7 current in freshly isolated SAN and assessed whether TRPM7 is efficiently deleted in SAN cells of $KO^{\alpha MHC\text{-}Cre}$ mice. We first confirmed robust Cre expression in all observed SAN cells by crossing α*MHC-Cre* mice with the *mT/mG* reporter mouse line ($ROSA26^{mTmG}$), in which membrane-targeted green fluorescent protein expression (*mG*) is induced only after *Cre*-mediated recombination (14) (Fig. 4*A*, single SAN shown). Indeed, α*MHC-Cre* induces recombination in all myocardial cells (15). Next we confirmed deletion of *Trpm7* exon 17 from genomic DNA isolated from SAN by PCR in $KO^{\alpha MHC\text{-}Cre}$ mice (Fig. 4*B*) according to the presence of the expected size of the deletion product. Finally we measured TRPM7 current from isolated SAN ($I_{Trpm7,\ \text{WT SAN}} = 32.0 \pm 6.2$ pA/pF at +100 mV, $n = 6$) and found them to be ~fourfold larger than TRPM7 in AVM ($I_{Trpm7,\ \text{AVM}} = 8.3 \pm 0.9$ pA/pF, $n = 5$) and absent in $KO^{\alpha MHC\text{-}Cre}$ SAN ($I_{Trpm7,\ \text{KO SAN}} = 0.4 \pm 0.2$ pA/pF, $n = 4$, $P < 0.01$; Fig. 4 *C* and *D*). Similar to EVM, the initial TRPM7 current on break-in before SAN dialysis is negligible and

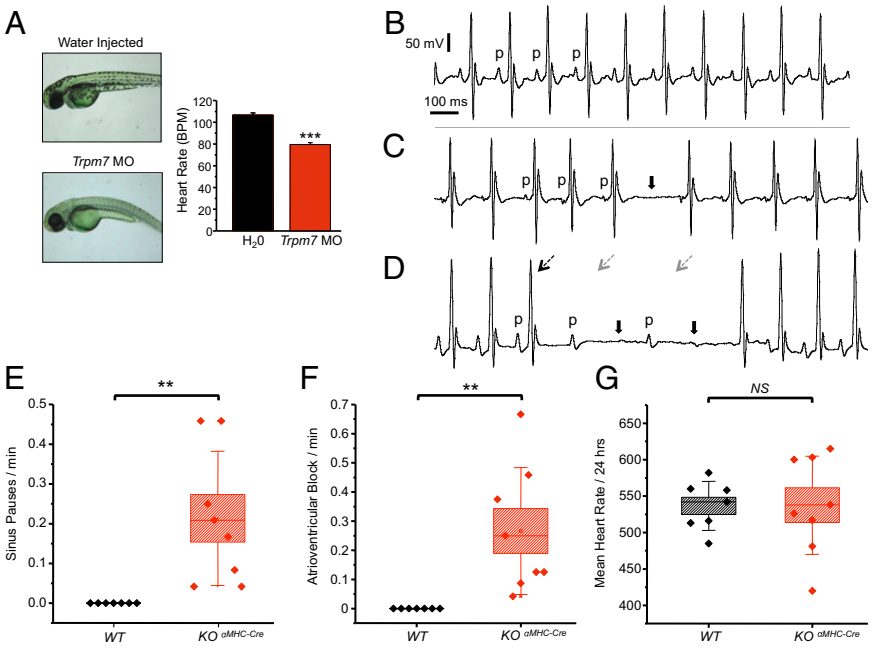

Fig. 3. *Trpm7* deletion in vivo disrupts automaticity in zebrafish and induces SPs and AVB in mice. (*A*) (*Left*) Images of zebrafish embryos: water-injected (*Upper*) and *Trpm7* MO-injected (*Lower*). (*Right*) *Trpm7* MO zebrafish ($n = 30$) and water-injected zebrafish ($n = 27$) heart rates. (*B*) Normal sinus rhythm (p denotes P waves; atrial depolarization) with intact atrioventricular conduction in the ECG of a telemetered, conscious *WT* mouse. (*C*) Representative ECG showing an episode of SP observed in a $KO^{\alpha MHC\text{-}Cre}$ mouse. Solid arrows denote location of expected p waves. (*D*) Representative ECGs demonstrating AVB observed in $KO^{\alpha MHC\text{-}Cre}$ mice (broken black arrow, conducted QRS complexes; broken gray arrow, expected location of QRS complex). (*E* and *F*) Box plots with overlying data points showing the distribution of the frequency of (*E*) SPs and (*F*) AVB observed over 24 h of telemetric monitoring in *WT* ($n = 7$) and $KO^{\alpha MHC\text{-}Cre}$ ($n = 8$) mice. (*G*) Mean heart rates of *WT* and $KO^{\alpha MHC\text{-}Cre}$ over a 24-h period were not statistically different. In box plots, error bars represent the SD of the mean. Box height represents the SE. $^{**}P < 0.01$, $^{***}P < 0.001$.

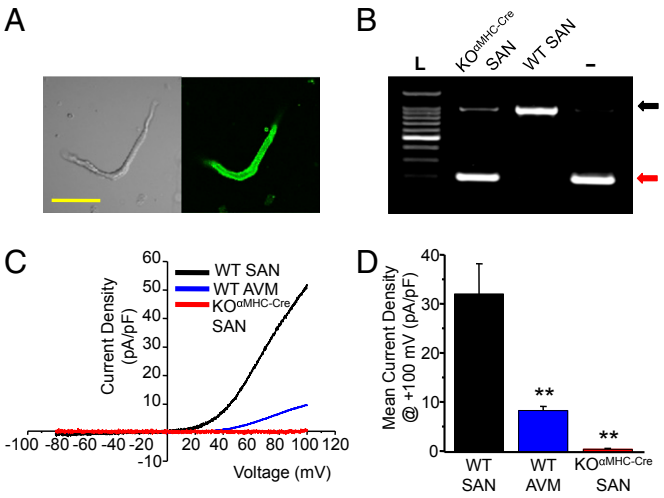

Fig. 4. TRPM7 is highly expressed in murine SAN. (*A*) Confocal images of an isolated SAN freshly dissociated from adult *αMHC-Cre-ROSA26*^{mTmG} heart: differential interference contrast (*Left*) and fluorescence GFP image (*Right*). (Scale bar, 50 μm.) (*B*) PCR across exon 17 from genomic DNA isolated from dissected *KO*$^{αMHC\text{-}Cre}$ and *WT* SAN. Tail DNA from *Trpm7*$^{fl/-}$ (-) serves as a positive control for *Trpm7* exon 17 deletion. Black arrow, full-length exon 17. Red arrow, deleted exon 17. (*C*) Representative TRPM7 current-voltage traces measured in *WT* SAN, *WT* AVM, and *KO*$^{αMHC\text{-}Cre}$ SAN. (*D*) Mean TRPM7 current density in *WT* SAN ($I_{Trpm7,\ WT\ SAN}$ = 32.0 ± 6.2 pA/pF, n = 6), *WT* AVM ($I_{Trpm7,\ AVM}$ = 8.3 ± 0.9 pA/pF, n = 5), and SAN ($I_{Trpm7,\ KO\alpha MHC\text{-}Cre\ SAN}$ = 0.4 ± 0.2 pA/pF, n = 4, P < 0.01).

only activates fully after ∼10 min of cell dialysis (Fig. S4). Thus, measuring TRPM7 current in SAN, under these conditions, serves primarily as an assay to quantify the amount of functional TRPM7 channels in the membrane of a given cell, as opposed to showing the active current present under physiological conditions.

As with EVM, we next assessed automaticity in *WT* (Fig. 5*A*) and *KO*$^{αMHC\text{-}Cre}$ SAN (Fig. 5*B*) using confocal microscopy to measure spontaneous Ca^{2+} transients. Ca^{2+} transient frequency is significantly diminished in *KO*$^{αMHC\text{-}Cre}$ SAN (Ca^{2+} transient rate $_{KO}$ = 32 ± 5 /min, n = 34) compared with *WT* (Ca^{2+} transient rate $_{WT}$ = 72 ± 11, n = 26, P < 0.01; Fig. 5*C*), and Ca^{2+} transients are lengthened (Fig. 5*D*), as observed in TRPM7-depleted EVM (Fig. 2). Isoproterenol (ISO) increases the Ca^{2+} transient frequency in both *WT* and *KO*$^{αMHC\text{-}Cre}$ cells, but the maximal rate reached by *KO*$^{αMHC\text{-}Cre}$ cells in ISO remains slower than in *WT* counterparts. Similar results, although less marked, are obtained by measuring the frequency of Ca^{2+} transients in individual pacemaker cells within the intact, undissociated SAN upon TRPM7 deletion (Fig. S5*A*). Despite these clear differences in Ca^{2+} transient firing frequency, peak Ca^{2+} transients are no different in *KO*$^{αMHC\text{-}Cre}$ SAN compared with *WT* (Fig. S5*B*), consistent with unchanged SR Ca^{2+} load as assessed by 10 mM caffeine application (Fig. S5*C*).

Cardiac automaticity is determined by diastolic depolarization arising from the combined effects of voltage-gated ion channels (*Hcn2*/*Hcn4*/$Ca_v3.1$/$Ca_v1.3$) and intracellular Ca^{2+} cycling (diastolic Ca^{2+} and *Ncx2*) (3). Thus we next measured the rate of rise of diastolic Ca^{2+} leading up to each Ca^{2+} transient and found this to be significantly blunted in *KO*$^{αMHC\text{-}Cre}$ SAN (Fig. 5*E*, *Right*) compared with *WT* (Fig. 5*E*, *Left*) and also only minimally responsive to ISO stimulation (Fig. 5*F*). These data suggest that TRPM7 is required for maintenance of normal automaticity in murine SAN and that it can influence diastolic Ca^{2+} release, either directly or indirectly, and thereby contribute to diastolic depolarization in SAN (3).

DDSL Is Diminished in *KO*$^{αMHC\text{-}Cre}$ SAN Cells: *Hcn4* and I_f Are Down-Regulated. To further examine the mechanism by which *Trpm7* deletion impairs SAN cell automaticity we measured spontaneous action potentials (APs) in freshly isolated SAN using the perforated patch-clamp technique. Consistent with the Ca^{2+} imaging experiments, AP firing rates are significantly diminished in *KO*$^{αMHC\text{-}Cre}$ SAN compared with *WT* SAN (Fig. 6 *A* and *B*) and largely reversed by ISO. By measuring membrane potential, we quantified the DDSL (Fig. 6*C*), an important determinant of SAN firing rate (4), in *WT* and *KO*$^{αMHC\text{-}Cre}$ SAN. DDSL was significantly lower in *KO*$^{αMHC\text{-}Cre}$ (DDSL $_{KO}$ = 0.03 ± 0.01 mV/ms, n = 5, P < 0.05) compared with WT (DDSL $_{WT}$ = 0.09 mV/ms ± 0.01, n = 7), and this difference was reversed by 100 nM ISO (Fig. 6 *C* and *D* and Table S1).

Rising diastolic Ca^{2+} is thought to contribute, in part, to diastolic depolarization in SAN via forward mode Na^+-Ca^{2+} exchange current and calcium-induced Ca^{2+} release (3, 16), but other membrane currents, including the hyperpolarization-activated pacemaker current (I_f, encoded by *Hcn1*/*Hcn2*/*Hcn4*), T-type Ca^{2+} current ($I_{Ca,T}$, encoded by $Ca_v3.1$), and L-type Ca^{2+} current ($I_{Ca,L}$, encoded by $Ca_v1.3$/$Ca_v1.2$) (2–4, 17) also participate. In fact, acute blockade of I_f alone in isolated SAN, using the selective I_f blocker ivabradine (18), was recently shown to be capable of slowing intracellular Ca^{2+} cycling kinetics and prolonging the period of spontaneous local Ca^{2+} releases occurring during diastolic depolarization (19). Thus, much of what we observe with respect to Ca^{2+} cycling in *KO*$^{αMHC\text{-}Cre}$ SAN may be explained via a mechanism of *Hcn4* and I_f reduction. Accordingly, we examined the change in relative expression levels of a panel of genes implicated in cardiac automaticity, both in vitro in cultured *Trpm7*-deleted EVM as well as in dissected SAN from *WT* and *KO*$^{αMHC\text{-}Cre}$ hearts. In *Trpm7*-deleted EVM, *Hcn4*, $Ca_v3.1$, and *SERCA2a* mRNA are robustly down-regulated eightfold, sixfold, and sixfold respectively, relative to *WT* ECM, whereas *Trpm4*, *Hcn2*, and $Ca_v1.3$ are not significantly differentially expressed (Fig. 7*A*). As expected, *Trpm7* mRNA is 19-fold reduced in these *Trpm7*-deleted cells. Similarly, in SAN dissected from *KO*$^{αMHC\text{-}Cre}$ hearts, *Hcn4* mRNA is reduced twofold, and *Trpm7* mRNA is threefold reduced relative to *WT* SAN. However, neither *Hcn2*, *Trpm4*, $Ca_v3.1$, $Ca_v1.3$, nor *Serca2a* mRNA are significantly down-regulated in *KO*$^{αMHC\text{-}Cre}$ SAN (Fig. 7*B*). We next measured the hyperpolarization-activated current, I_f, in freshly isolated SAN to establish whether these reductions in *Hcn4* mRNA indeed result in diminished functional I_f current (Fig. 7 *C* and *D*). We find I_f to be on average significantly diminished in *KO*$^{αMHC\text{-}Cre}$ SAN ($I_{f,\ KO\alpha MHC\text{-}Cre}$ = −11.9 ± 2.6 pA/pF @ −160 mV, n = 27) compared with *WT* ($I_{f,\ WT}$ = −28.7 ± 6.6 pA/pF @ −160 mV, n = 14, P < 0.01). Furthermore, functional mosaicism is observed in which some *KO*$^{αMHC\text{-}Cre}$ SAN have virtually no I_f (9/27 = 33% < −3 pA/pF at −160 mV), whereas other *KO*$^{αMHC\text{-}Cre}$ SAN have nearly normal I_f current densities (Fig. 7*E*). On the other hand, no *WT* SAN (0 of 14) have I_f current densities below 3 pA/pF.

Because $Ca_v3.1$ mRNA is also significantly down-regulated upon *Trpm7* deletion in cultured EVM but not in isolated *KO*$^{αMHC\text{-}Cre}$ SAN, we examined whether L-type Ca^{2+} current ($I_{Ca,L}$) or T-type Ca^{2+} current ($I_{Ca,T}$) are altered in isolated *KO*$^{αMHC\text{-}Cre}$ SAN, because these currents are also thought to contribute to both diastolic Ca^{2+} influx and diastolic depolarization in SAN. We measured $I_{Ca,T}$ by subtracting $I_{Ca,L}$ (Fig. 7*F*, *Right*) from total Ca^{2+} current, $I_{Ca,T}$ + $I_{Ca,L}$ (Fig. 7*F*, *Left*) and generated the current–voltage relationship for $I_{Ca,T}$ shown in Fig. 7*G*. $I_{Ca,L}$, $I_{Ca,T}$ + $I_{Ca,L}$, and $I_{Ca,T}$ are not significantly different in *KO*$^{αMHC\text{-}Cre}$ compared with *WT* SAN at all membrane potentials examined. Collectively these data suggest that the negative chronotropic effects of *Trpm7* deletion in SAN are mediated largely via down-regulation of *Hcn4* and I_f, which decreases the slope of diastolic depolarization and thereby slows

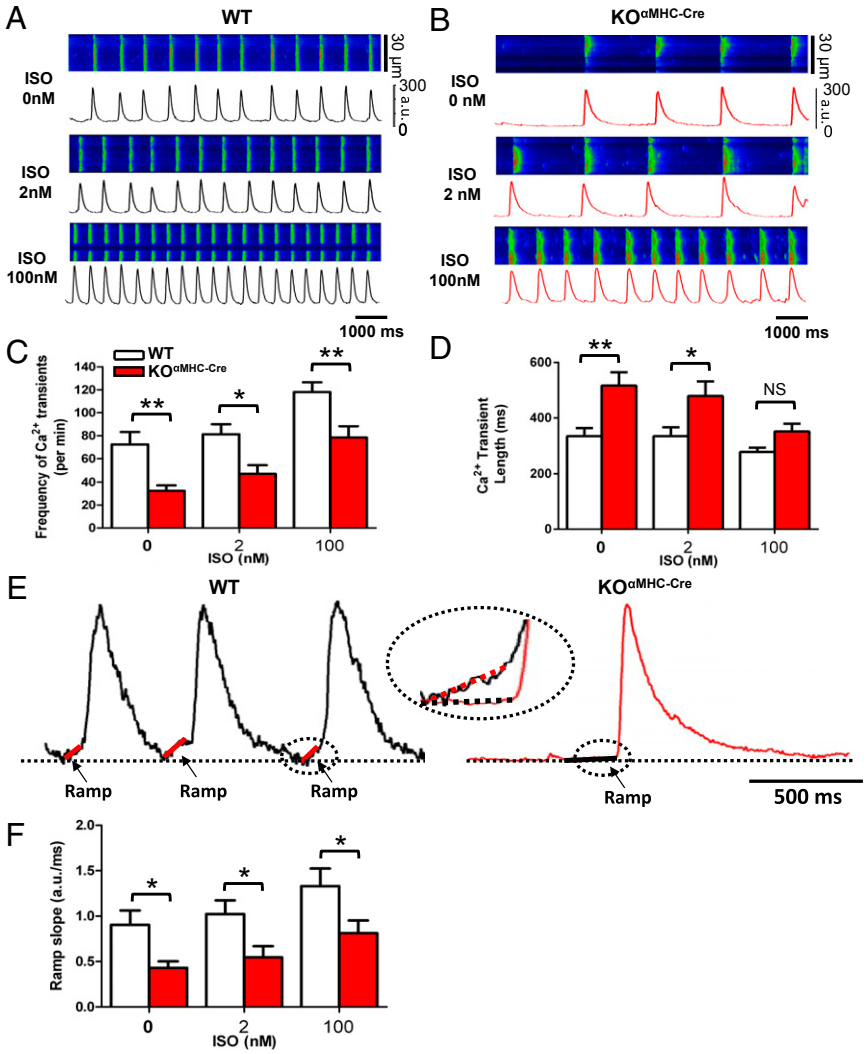

Fig. 5. *Trpm7* deleted SAN exhibit impaired automaticity with slowed diastolic Ca^{2+} rise. Ca^{2+} transients measured by high-speed line-scanning confocal microscopy in (*A*) *WT* SAN and (*B*) $KO^{\alpha MHC\text{-}Cre}$ SAN under basal conditions (*Top*) and after stimulation with ISO: 2 nM (*Middle*) and 100 nM (*Bottom*). (*C*) Mean Ca^{2+} transient frequency and (*D*) Ca^{2+} transient length in *WT* SAN compared with $KO^{\alpha MHC\text{-}Cre}$ SAN under basal conditions and after stimulation with 2 nM and 100 nM ISO. (*E*) Representative Ca^{2+} transients from *WT* (*Left*) and $KO^{\alpha MHC\text{-}Cre}$ (*Right*) showing the slope of diastolic Ca^{2+} rise (Ca^{2+} ramp). (*F*) Mean slope of the diastolic Ca^{2+} ramp in *WT* and $KO^{\alpha MHC\text{-}Cre}$ under increasing ISO concentrations. $^{*}P < 0.05$, $^{**}P < 0.01$.

automaticity. Consistent with this notion, $KO^{\alpha MHC\text{-}Cre}$ mice are less sensitive than *WT* counterparts, in a dose-dependent fashion, to the negative chronotropic effects of the ivabradine (Fig. 7*H*). Furthermore, the recently identified TRPM7 blocker FTY720 has no effect on SAN firing rates and AP durations when acutely applied to WT SAN cells at a concentration shown to nearly completely block endogenous TRPM7 in human atrial fibroblasts (500 nM) (20) (Fig. S6).

Postdevelopmental, SAN-Restricted *Trpm7* Deletion Recapitulates the Phenotype Observed in $KO^{\alpha MHC\text{-}Cre}$ Mice. Because α*MHC-Cre* is expressed and recombines in cardiomyocytes as early as E12–14 (21), it is possible that these findings in adult $KO^{\alpha MHC\text{-}Cre}$ SAN result from developmental effects of *Trpm7* on SAN maturation or differentiation, consistent with our previous findings in lymphocytes (7) and embryonic tissues (15, 22). Furthermore, α*MHC-Cre* deletes globally in heart, so it is also conceivable that $KO^{\alpha MHC\text{-}Cre}$ SAN are affected in a paracrine fashion by *Trpm7* deletion in neighboring, non-SAN cells. To address these alternative mechanisms, we crossed *Hcn4-CreERT2* mice (23) with $Trpm7^{fl/fl}$ or $Trpm7^{fl/-}$ mice to generate a line of mice ($KO^{Hcn4\text{-}CreERT2}$) that provides tamoxifen (*Tm*)-inducible, SAN/AVN-restricted *Trpm7* deletion (Fig. 8*A*). Using *Hcn4-CreERT2-ROSA26*^{mTmG} mice, we demonstrate efficient recombination that is restricted to the SAN region (green, mGFP) in 6-wk-old *Hcn4-CreERT2-ROSA26*^{mTmG} mouse right atrium (red, mTomato) (Fig. 8*B*) after *Tm* gavage (40 mg/kg) × 4 d (Fig. 8*A*). In addition, genomic DNA isolated from $KO^{Hcn4\text{-}CreERT2}$ SAN reveals efficient deletion of *Trpm7* exon 17 according to the presence of the expected size of the deletion product on PCR (Fig. 8*C*). Finally, TRPM7 current measured by whole-cell patch clamp of $KO^{Hcn4\text{-}CreERT2}$ SAN is eliminated ($I_{Trpm7,\ KO,Hcn4\text{-}CreERT2\ \mathrm{SAN}} = 0.1 \pm 0.1$ pA/pF, $n = 4$, $P < 0.01$; Fig. 8 *D* and *E*). Having established effective, postdevelopmental, SAN-restricted *Trpm7* deletion in $KO^{Hcn4\text{-}CreERT2}$ mice, we next performed telemetric studies to assess for bradyarrhythmias, as observed in $KO^{\alpha MHC\text{-}Cre}$ mice. Strikingly, $KO^{Hcn4\text{-}CreERT2}$ mice also exhibit SPs with ectopic atrial escape rhythms (Fig. 8 *F* and *G*, *Left*) as well as AVB (Fig. 8*G*, *Right*), whereas the mean heart rate over 24 h is unchanged, similar to $KO^{\alpha MHC\text{-}Cre}$ (Fig. 3 *C*–*F* and Fig. S3). Likewise, I_f in patch-clamped $KO^{Hcn4\text{-}CreERT2}$ SAN is significantly diminished ($I_{f,\ KOHcn4\text{-}CreERT2} = -6.9 \pm 2.2$ pA/pF, $n = 25$) relative to *WT*

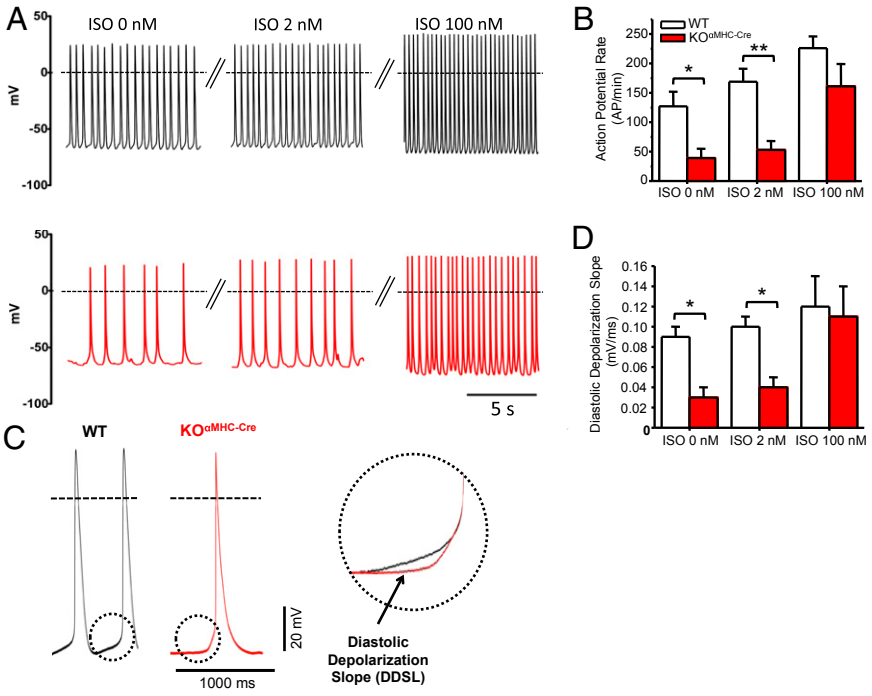

Fig. 6. *Trpm7* deletion slows spontaneous AP firing and diastolic depolarization in murine SAN. (*A*) Spontaneous APs recorded in *WT* SAN (*Upper*) and $KO^{\alpha MHC\text{-}Cre}$ SAN (*Lower*) under basal conditions (*Left*), 2 nM ISO (*Center*), and 100 nM ISO (*Right*). (*B*) Mean AP firing rate. (*C*) Representative AP from *WT* SAN compared with $KO^{\alpha MHC\text{-}Cre}$ SAN showing slowed DDSL in $KO^{\alpha MHC\text{-}Cre}$ SAN. (*D*) Mean DDSL in *WT* SAN compared with $KO^{\alpha MHC\text{-}Cre}$ SAN under basal conditions and with 2 nM and 100 nM ISO. $^*P < 0.05$, $^{**}P < 0.01$.

SAN ($I_{f,\ WT\ SAN} = -21.8 \pm 4.9$ pA/pF, $n = 11$, $P < 0.01$, Fig. 8 *H* and *I*) and comparable to $KO^{\alpha MHC\text{-}Cre}$ ($I_{f,\ KO\alpha MHC\text{-}Cre} = -11.9 \pm 2.6$ pA/pF @ −160 mV, $n = 27$, $P = 0.14$ compared with $I_{f,\ KOHcn4\text{-}CreERT2}$). Also similar to $KO^{\alpha MHC\text{-}Cre}$ SAN was the percentage of $KO^{Hcn4\text{-}CreERT2}$ SAN with near-zero I_f amplitudes (14 of 25 or 56% < −3 pA/pF at −160 mV) vs. (0 of 11) in *WT* SAN. Taken together, these data show that *Trpm7* is required for the maintenance of normal cardiac automaticity via transcriptional regulation of *Hcn4* and I_f in adult murine SAN and embryonic myocardium.

Discussion

We sought to determine the contribution of TRPM7 to myocardial function by studying the consequences of cardiac-targeted *Trpm7* deletion in vitro and in vivo. We show that TRPM7, when activated, forms a significant outwardly rectifying current in several different myocardial subtypes: with highest current densities in EVM > SAN > AVM. TRPM7 deletion in cultured EVM slows cardiac automaticity in vitro, as does *TRPM7* knockdown in zebrafish. Moreover, in both global cardiac ($KO^{\alpha MHC\text{-}Cre}$) and inducible SAN-restricted ($KO^{Hcn4\text{-}CreERT2}$), TRPM7 deletion disrupts automaticity of isolated SAN and intact SAN (and likely AVN), manifesting as SPs and AVB in the adult mouse heart. Given that TRPM7 is known to conduct Ca^{2+} (8), an obvious potential mechanism is that TRPM7 provides a Ca^{2+} influx pathway important for cardiac automaticity. However, it important to note that TRPM7 currents are typically recorded under nonphysiological conditions, becoming fully activated after ∼10 min of cell dialysis (i.e., Mg^{2+} chelation with EDTA/Na_2ATP), in nominally free external Mg^{2+}. Under these conditions, TRPM7 current density is used to assay the total amount of functional protein at the cell membrane as opposed to physiologically relevant current magnitudes. Under more physiological conditions, TRPM7 current is essentially inactive in SAN and EVM, as demonstrated by the initial currents on "break-in" (Figs. S1 and S4). Thus, it is unlikely that TRPM7 contributes in a meaningful way to diastolic Ca^{2+} influx, under basal conditions, given the strong outward rectification characteristic of TRPM7 and its further inhibition by physiological concentrations of extracellular Mg^{2+}. Finally, TRPM7 blockade using FTY720 had no effect on WT SAN firing rates under basal physiological conditions (Fig. S6).

There are a number of other ion channels, *Hcn4*, *Hcn2*, $Ca_v3.1$, and $Ca_v1.3$, nonetheless, that are considered important for cardiac automaticity (4). Indeed, expression analysis for these "automaticity" genes revealed significant reductions in *Hcn4*, $Ca_v3.1$, and *SERCA2a* mRNA in EVM upon TRPM7 deletion, whereas in SAN only *Hcn4* mRNA was reduced. Consistent with these findings, the pacemaker current, I_f (encoded by *Hcn4*), is significantly reduced in isolated SAN and associated with slowed diastolic depolarization. Furthermore, $KO^{\alpha MHC\text{-}Cre}$ mice were less sensitive than *WT* mice to the negative chronotropic effects of the I_f blocker ivabradine. Thus we conclude that TRPM7 is required for maintenance of cardiac automaticity via transcriptional regulation of *Hcn4* expression (via an as yet unidentified pathway).

It is well established that the hyperpolarization-activated pacemaker current, I_f, (encoded by *Hcn4*) contributes to basal automaticity in mouse SAN (24–26) and embryonic heart (27). However, there is controversy as to the extent of this contribution. *Hcn4* knockout studies have demonstrated phenotypes ranging from profound bradycardia with AV block (24) to modest SPs (25), with no significant effect on mean heart rates in telemetered mice, similar to what we observe. Also consistent with our results, both of these studies show clear effects on firing rates and diastolic depolarization of isolated SAN cells. Furthermore, with maximal β-adrenergic stimulation (100 nM ISO), $KO^{\alpha MHC\text{-}Cre}$ SAN largely overcome impairments in automaticity. This finding is consistent with the notion that I_f current is an important determinant of spontaneous activity under basal conditions (25) but does not play an exclusive role in β-adrenergic

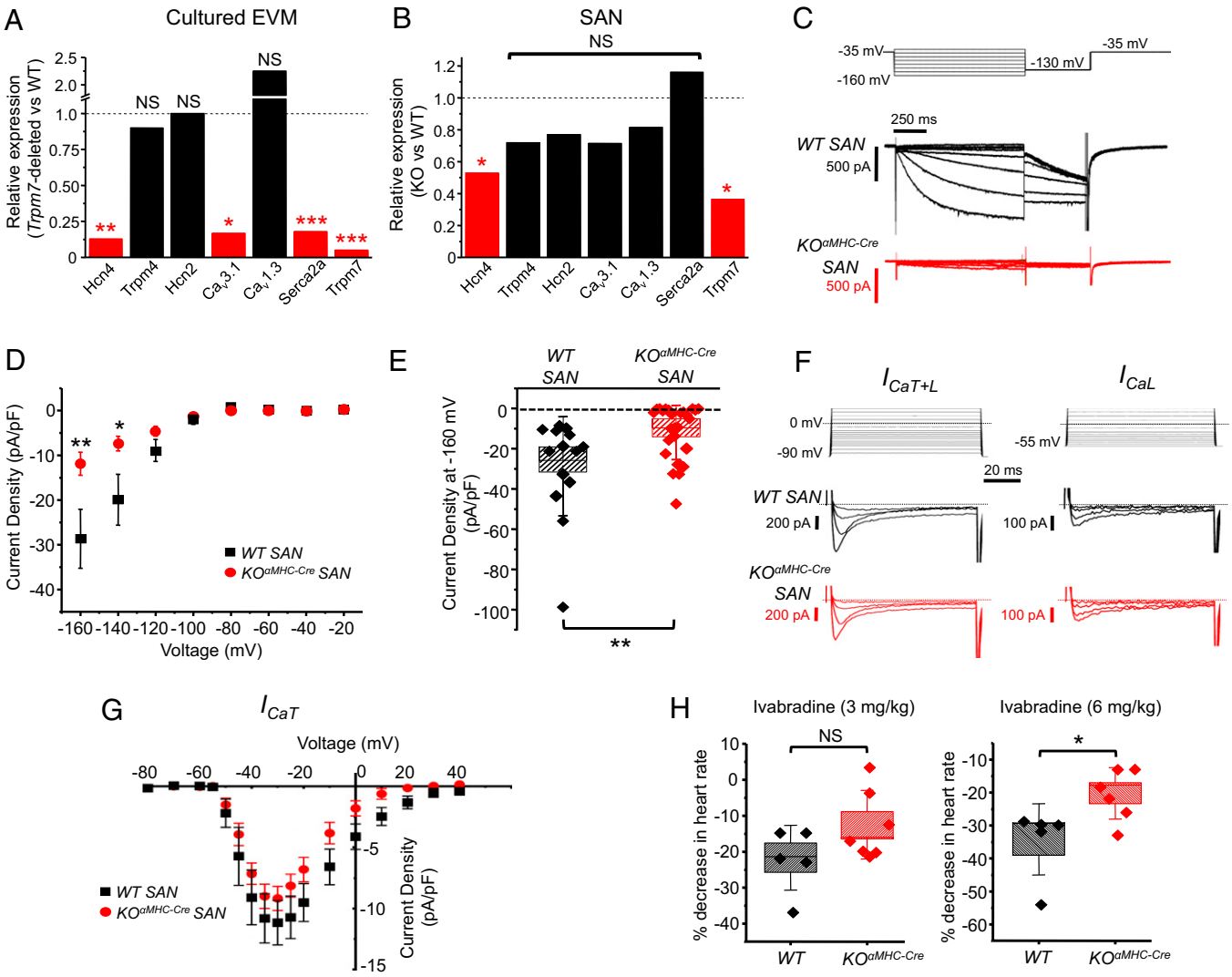

Fig. 7. *Hcn4* mRNA and pacemaker current are down-regulated upon *Trpm7*-deletion in EVM and SAN cells. mRNA expression profile of genes implicated in automaticity in (*A*) cultured *Trpm7*-deleted EVM (n = 10 samples: 6 *Ad*-TnT-Cre and 4 *Ad*-CMV-Cre) relative to *WT* EVM (n = 5 samples: *Ad*-Lacz-Cre) and in (*B*) $KO^{\alpha MHC\text{-}Cre}$ (n = 4 samples, 4–6 pooled SAN/sample) relative to *WT* SAN (n = 3 samples, 4–6 pooled SAN/sample). (*C*) Representative hyperpolarization-activated "funny" current traces, I_f, from *WT* SAN (*Middle*) and $KO^{\alpha MHC\text{-}Cre}$ SAN (*Bottom*). Voltage protocols are shown above current traces. (*D*) I_f current–voltage relationship from *WT* SAN (n = 14) compared with $KO^{\alpha MHC\text{-}Cre}$ SAN (n = 27). (*E*) Box plots with overlying data points showing the mean and distribution of I_f current densities at −160 mV from *WT* SAN (n = 14) compared with $KO^{\alpha MHC\text{-}Cre}$ SAN (n = 27). (*F*) Representative Ca^{2+} current traces of total Ca^{2+} (I_{CaT+L}, *Left*) and L-type Ca^{2+} current ($I_{Ca,L}$, *Right*) from *WT* SAN (*Middle*) and $KO^{\alpha MHC\text{-}Cre}$ SAN (*Bottom*). Voltage protocols are shown above current traces. (*G*) Current–voltage relationship of T-type Ca^{2+} currents ($I_{Ca,T}$: obtained by subtracting $I_{Ca,L}$ from I_{CaT+L}) from *WT* SAN (n = 6) compared with $KO^{\alpha MHC\text{-}Cre}$ SAN (n = 10). (*H*) Box plots with overlying data points showing the mean and distribution of heart rates after ivabradine (*Left*: 3 mg/kg; *Right*: 6 mg/kg) in *WT* mice (n = 5) compared with $KO^{\alpha MHC\text{-}Cre}$ mice (n = 7). In box plots error bars represent the SD of the mean. Box height represents the SE. In current–voltage relationships, error bars represent SEs. Statistical significance in *A* and *B* are based on ΔC_t values (C_t of gene − C_t GAPDH) and SD for each gene in *Trpm7*-deleted or KO compared with WT, using an unpaired Student t test. $^*P < 0.05$, $^{**}P < 0.01$, $^{***}P < 0.001$.

regulation of pacemaking (26). With β-adrenergic stimulation, the membrane potential rises during late depolarization, and I_f contributes less, allowing other ionic mechanisms, such as $Ca_v3.1$, $Ca_v1.3$, and SR Ca^{2+} release, to dominate. It is also noteworthy that in both $KO^{\alpha MHC\text{-}Cre}$ and $KO^{Hcn4\text{-}CreERT2}$ mice, I_f is reduced in a mosaic fashion such that there is a small population of SAN cells that contain near-normal I_f current densities. Therefore, the *KO* phenotype of SPs with no significant change in mean HR over 24 h is consistent with a mechanism in which a population of SAN cells, with near-normal I_f, supports "normal" automaticity by overdrive pacing the I_f-deficient SAN cells. However, given the lower number of "normal" SAN cells, this overdrive pacing occasionally fails and results in SPs.

Another member of the TRPM family, *Trpm4*, has been recently found to be mutated in forms of conduction system disease in humans, including progressive familial heart block I (28, 29). These are thought to be gain-of-function mutations resulting in impaired TRPM4 endocytosis secondary to constitutive SUMOylation. The mechanism for this gain of function was deduced on the basis of heterologous expression studies in HEK cells and the observation that TRPM4 is enriched in human (28) and bovine (29) Purkinje cells. However, the mechanisms underlying TRPM4 gain-of-function contributions to conduction block has yet to be established. Because TRPM4 is a Ca^{2+}-activated, sodium-selective current, one possibility is that increased TRPM4 current density results in further membrane depolarization in Purkinje cells, inactivating excitatory voltage-

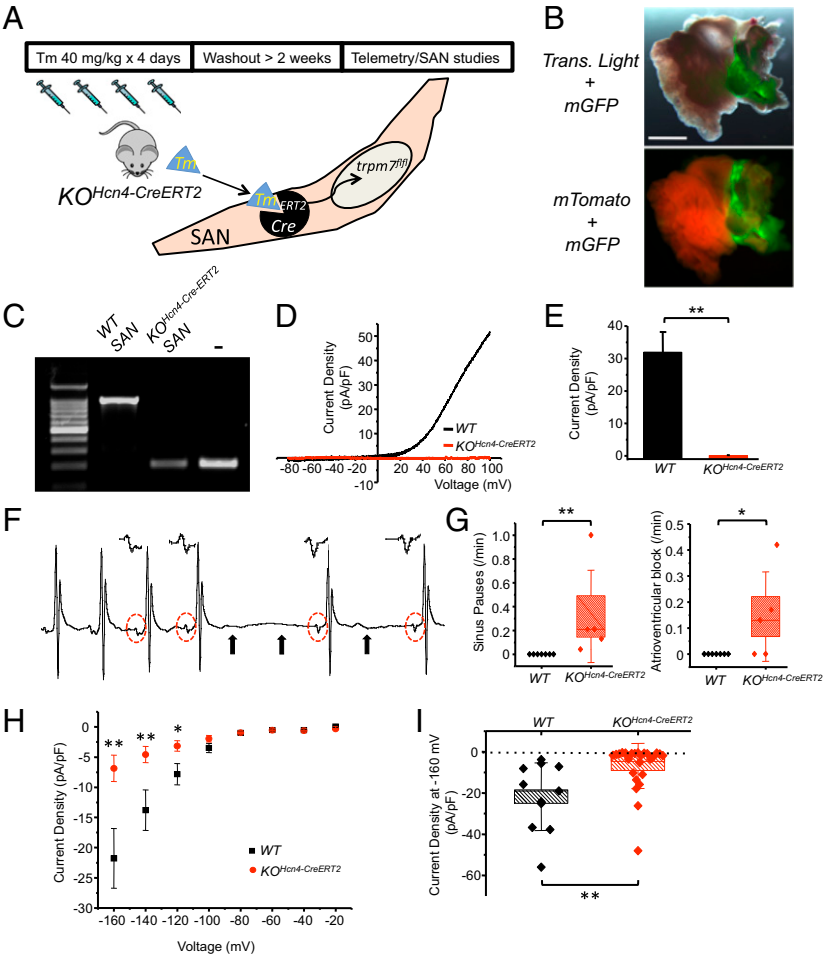

Fig. 8. Postnatal SAN/AVN restricted *Trpm7* deletion recapitulates the phenotype of global cardiac *Trpm7 KO*. (*A*) SAN-restricted *Trpm7* deletion ($KO^{Hcn4\text{-}CreERT2}$) was achieved in *Hcn4-CreERT2* × $Trpm7^{fl/fl}$/$Trpm7^{fl/-}$ mice at 6–8 wk of age by treating with tamoxifen (40 mg/kg) by gavage for 4 d, followed by >2-wk washout period before telemetry and SAN studies (*B*) (*Upper*) Transmitted light + GFP fluorescence image of *Hcn4-CreERT2-ROSA26*^{mTmG} right atrium after tamoxifen treatment. (*Lower*) Fluorescence mTomato/mGFP image showing recombination (mGFP) restricted to SAN region. (Scale bar, 1 mm.) (*C*) PCR across exon 17 from genomic DNA isolated from dissected $KO^{Hcn4\text{-}CreERT2}$ and *WT* SAN. Tail DNA from $Trpm7^{fl/-}$ serves as a positive control for *Trpm7* exon 17 deletion (-). (*D*) Representative TRPM7 current–voltage traces measured in *WT* SAN and $KO^{Hcn4\text{-}CreERT2}$ SAN. (*E*) Mean TRPM7 current density in *WT* SAN and $KO^{Hcn4\text{-}CreERT2}$ SAN. (*F*) Representative ECG showing an episode of SP observed in a telemetered $KO^{Hcn4\text{-}CreERT2}$ mouse. Solid arrows denote location of expected p waves. Red dashed circles and *Insets* above show change in p-wave morphology after SP, indicative of ectopic atrial focus. (*G*) Box plots with overlying data points showing the distribution of the frequency SPs (*Left*) and AVB (*Right*) observed over 24 h of telemetric monitoring in *WT* ($n = 7$) and $KO^{Hcn4\text{-}CreERT2}$ ($n = 5$) mice. (*H*) I_f current–voltage relationship from *WT* SAN ($n = 11$) compared with $KO^{Hcn4\text{-}CreERT2}$ SAN ($n = 25$). (*I*) Box plots with overlying data points showing the mean and distribution of I_f current densities at −160 mV from *WT* SAN ($n = 11$) compared with $KO^{Hcn4\text{-}CreERT2}$ SAN ($n = 25$). $^*P < 0.05$, $^{**}P < 0.01$.

gated ionic currents and reducing the contribution of hyperpolarization-activated currents (I_f) (28). To date, no gain-of-function mouse model data are available, and the $Trpm4^{-/-}$ mouse, aside from hypertension (30), has not yet been shown to develop other cardiovascular phenotypes.

This article reports a TRP channel influencing the expression level of another ion channel(s) in SAN and EVM. The connection between TRPM7 and *Hcn4* expression in SAN and EVM remains an intriguing question. We showed recently that TRPM7 is required for early events in cardiogenesis, and perturbations in TRPM7 function during ventricular development impair myocardial function, atrioventricular conduction, and repolarization (15). Thus, we surmised that embryonic deletion of TRPM7 in SAN/AVN tissue in $KO^{\alpha MHC\text{-}Cre}$ mice might alter the maturation of SAN/AVN cells and consequently the expression of *Hcn4*. However, SAN/AVN-restricted TRPM7 deletion in *adult* $KO^{Hcn4\text{-}CreERT2}$ mice recapitulated the phenotype observed in $KO^{\alpha MHC\text{-}Cre}$ mice, suggesting that the effect of TRPM7 on *Hcn4* expression and automaticity in SAN represents, instead, a post-developmental effect. In this regard, it is noteworthy that SAN cells are more fetal-like, in that they are smaller, mononucleated, and retain automaticity, similar to early embryonic myocardium and in contrast to the larger, quiescent, multinucleated adult ventricular cells. Perhaps it is retention of this "embryonic" nature of SAN cells that allows them to remain sensitive to the effects of TRPM7 after the developmental phase.

A number of studies now show that the T-box transcription factor *Tbx3* is critical in mediating the developmental programs leading to formation and function of SAN, AVN, and conduction system in murine heart (31–34). Indeed, the most marked differentially expressed gene upon manipulation of *Tbx3* expression levels in myocardium is *Hcn4* (33). In addition, *Tbx3*-deficient mice exhibit both SAN and AVN dysfunction, manifested as SPs and AVB, respectively (35). *Mef2* transcription factors have also been shown to directly regulate *Hcn4* expression (36), and the $Mef2a^{-/-}$ mouse develops sinus arrhythmia and conduction block (37). We speculate that *TRPM7* may influence these transcriptional pathways in heart, either directly or indirectly, to affect

cellular differentiation. We showed recently that TRPM7 C-terminal kinase is cleaved from the channel in LN-18 cells undergoing Fas-induced apoptosis, and this cleavage induced an increase in TRPM7 channel activity that is required for apoptosis (38). Indeed, cleaved TRPM7 C-terminal kinase has been observed in other cell types (38), potentially freeing it to interact with cellular partners beyond the plasma membrane to modify transcriptional programs. We are currently testing these hypotheses.

In summary, we showed that TRPM7 is most highly expressed in EVM and SAN myocytes, and genetic ablation of *Trpm7* in these cells severely disrupts automaticity in vitro and in vivo. Impaired automaticity in *Trpm7*-deleted murine SAN cells arises from a lower and flatter slope of diastolic depolarization, associated with a slowed diastolic Ca^{2+} rise and reduced pacemaker current I_f (encoded by *Hcn4*). The next goal will be to determine how TRPM7 transcriptionally regulates genes in SAN and in embryonic myocardium to affect cardiac automaticity.

Methods

Refer to *SI Methods* for full methods.

Cardiac-Targeted *Trpm7* Knockout Mice. All animal procedures have been reviewed and approved by the Institutional Animal Care and Use Committee at Children's Hospital Boston. Animals were housed under standard conditions and allowed access to food and water ad libitum. Cardiac-targeted knockout mice were generated by crossing $Trpm7^{fl/fl}$ and $Trpm7^{fl/-}$ mice described previously (7) with *αMHC-Cre* or *Hcn4-Cre-ERT2* (23) mice. Mice were maintained on 129/SvEvTac mixed genetic background.

Embryonic Cardiomyocyte Isolation, Culture, and Adenoviral Transduction. $Trpm7^{fl/fl}$ embryonic hearts (6–11) were removed from E13.5–14.0 embryos obtained from pregnant $Trpm7^{fl/fl}$ female mice mated with a $Trpm7^{fl/fl}$ male. Adenoviruses, *Ad-CMV-Lacz*, *Ad-CMV-Cre*, and *Ad-TnT-Cre*, were kind gifts from William Pu, Boston Children's Hospital, Boston, MA. EVM were incubated differentiation media (DM) with adenovirus (multiplicity of infection 100) for 24 h and then washed two times with DM. Experiments were performed 2–5 d after viral transduction.

Ventricular Cardiomyocyte Isolation. Ventricular myocytes were isolated by enzymatic digestion using either a solution of 0.07 mg/mL Liberase Blendzyme (Roche Diagnostics) or a mixture of 0.4 mg/mL Collagenase B (Roche), 0.3 mg/mL Collagenase D (Roche), and 0.025–0.05 mg/mL Protease XVI (Sigma), in nominally Ca^{2+}-free Tyrode's solution, as previously described (39).

Isolation of SAN Myocytes. SAN myocytes were isolated as described by Marger et al. (40).

Zebrafish Morpholino. Disruption of TRPM7 in zebrafish by MO injection was performed as previously described (41).

Ca^{2+} Imaging of Embryonic Cardiomyocytes. EVMs plated on 10-mm glass-bottom coverslip culture dishes were loaded with 5–10 μM Fluo-4 for 30 min at 37 °C in DM. The cells were imaged using an FV1000 confocal microscope.

Ca^{2+} Imaging of SAN Myocytes. Spontaneous $[Ca^{2+}]_i$ transients were recorded in both enzymatically isolated primary SAN cells and in individual cells of intact SAN tissue loaded with Fluo-4AM under control (Tyrode's) or ISO at 36 °C as previously described (42).

Mouse Telemetry. Mouse telemetry was performed as described previously (42).

Cellular Electrophysiology. I_{Trpm7}, I_f, I_{CaL}, and I_{CaT} were measured in the whole-cell configuration as previously described (7, 40). Cellular automaticity was recorded under perforated-patch conditions using β-escin as previously described (40).

Quantitative RT-PCR Expression Analysis. mRNA was quantified by quantitative RT-PCR from total RNA isolated from pooled SAN (four to six SAN per sample) dissected from *KO* or *WT* hearts, or from 35-mm dishes of beating cultured embryonic ventricular myocytes, as previously described (7).

Statistics. All data are represented as means ± SEM, unless otherwise specified. All *P* values were calculated using the two-samples, independent Student *t* test, with the exception of the data from Fig. 3 *E* and *F* and Fig. 8*G*, which used the nonparametric Mann-Whitney test.

ACKNOWLEDGMENTS. We thank Dr. William T. Pu for generously providing *Ad-Lacz*, *Ad-CMV-Cre*, and *Ad-TnT-Cre* adenoviruses. This study was supported by Ageance Nationale pour la Recherche (ANR) Grants ANR-2010-BLAN-1128-01 and ANR-09-GENO-034 (to M.E.M.). R.S. was supported by grants from the Leadership Council in Cardiovascular Care and the American Heart Association Fellow-to-Faculty transition award. The Intitut de Genomique Fonctionnelle group is a member of the Laboratory of Excellence, Ion Channel Science and Therapeutics, and is supported by a grant from ANR.

1. Gillis AM, et al.; Heart Rhythm Society; American College of Cardiology Foundation (2012) HRS/ACCF expert consensus statement on pacemaker device and mode selection. Developed in partnership between the Heart Rhythm Society (HRS) and the American College of Cardiology Foundation (ACCF) and in collaboration with the Society of Thoracic Surgeons. *Heart Rhythm* 9(8):1344–1365.
2. DiFrancesco D (2010) The role of the funny current in pacemaker activity. *Circ Res* 106(3):434–446.
3. Lakatta EG, Maltsev VA, Vinogradova TM (2010) A coupled SYSTEM of intracellular Ca2+ clocks and surface membrane voltage clocks controls the timekeeping mechanism of the heart's pacemaker. *Circ Res* 106(4):659–673.
4. Mangoni ME, Nargeot J (2008) Genesis and regulation of the heart automaticity. *Physiol Rev* 88(3):919–982.
5. Kunert-Keil C, Bisping F, Krüger J, Brinkmeier H (2006) Tissue-specific expression of TRP channel genes in the mouse and its variation in three different mouse strains. *BMC Genomics* 7:159.
6. Fonfria E, et al. (2006) Tissue distribution profiles of the human TRPM cation channel family. *J Recept Signal Transduct Res* 26(3):159–178.
7. Jin J, et al. (2008) Deletion of Trpm7 disrupts embryonic development and thymopoiesis without altering Mg2+ homeostasis. *Science* 322(5902):756–760.
8. Bates-Withers C, Sah R, Clapham DE (2011) TRPM7, the Mg(2+) inhibited channel and kinase. *Adv Exp Med Biol* 704:173–183.
9. Du J, et al. (2010) TRPM7-mediated Ca2+ signals confer fibrogenesis in human atrial fibrillation. *Circ Res* 106(5):992–1003.
10. Runnels LW, Yue L, Clapham DE (2002) The TRPM7 channel is inactivated by PIP(2) hydrolysis. *Nat Cell Biol* 4(5):329–336.
11. Zhang YH, et al. (2012) Evidence for functional expression of TRPM7 channels in human atrial myocytes. *Basic Res Cardiol* 107(5):282.
12. Arduini BL, Henion PD (2004) Melanophore sublineage-specific requirement for zebrafish touchtone during neural crest development. *Mech Dev* 121(11):1353–1364.
13. McNeill MS, et al. (2007) Cell death of melanophores in zebrafish trpm7 mutant embryos depends on melanin synthesis. *J Invest Dermatol* 127(8):2020–2030.
14. Muzumdar MD, Tasic B, Miyamichi K, Li L, Luo L (2007) A global double-fluorescent Cre reporter mouse. *Genesis* 45(9):593–605.
15. Sah R, et al. (2013) The timing of myocardial Trpm7 deletion during cardiogenesis variably disrupts adult ventricular function, conduction and repolarization. *Circulation* 128(2):101–114.
16. Hüser J, Blatter LA, Lipsius SL (2000) Intracellular Ca2+ release contributes to automaticity in cat atrial pacemaker cells. *J Physiol* 524(Pt 2):415–422.
17. Marionneau C, et al. (2005) Specific pattern of ionic channel gene expression associated with pacemaker activity in the mouse heart. *J Physiol* 562(Pt 1):223–234.
18. Thollon C, Vilaine JP (2010) I(f) inhibition in cardiovascular diseases. *Adv Pharmacol* 59:53–92.
19. Yaniv Y, et al. (2013) New evidence for coupled clock regulation of the normal automaticity of sinoatrial nodal pacemaker cells: Bradycardic effects of ivabradine are linked to suppression of intracellular Ca cycling. *J Mol Cell Cardiol* 62C:80–89.
20. Qin X, et al. (2013) Sphingosine and FTY720 are potent inhibitors of the transient receptor potential melastatin 7 (TRPM7) channels. *Br J Pharmacol* 168(6):1294–1312.
21. Gaussin V, et al. (2002) Endocardial cushion and myocardial defects after cardiac myocyte-specific conditional deletion of the bone morphogenetic protein receptor ALK3. *Proc Natl Acad Sci USA* 99(5):2878–2883.
22. Jin J, et al. (2012) The channel kinase, TRPM7, is required for early embryonic development. *Proc Natl Acad Sci USA* 109(5):E225–E233.
23. Herrmann S, Fabritz L, Layh B, Kirchhof P, Ludwig A (2011) Insights into sick sinus syndrome from an inducible mouse model. *Cardiovasc Res* 90(1):38–48.
24. Baruscotti M, et al. (2011) Deep bradycardia and heart block caused by inducible cardiac-specific knockout of the pacemaker channel gene Hcn4. *Proc Natl Acad Sci USA* 108(4):1705–1710.
25. Herrmann S, Stieber J, Stöckl G, Hofmann F, Ludwig A (2007) HCN4 provides a 'depolarization reserve' and is not required for heart rate acceleration in mice. *EMBO J* 26(21):4423–4432.
26. Alig J, et al. (2009) Control of heart rate by cAMP sensitivity of HCN channels. *Proc Natl Acad Sci USA* 106(29):12189–12194.
27. Stieber J, et al. (2003) The hyperpolarization-activated channel HCN4 is required for the generation of pacemaker action potentials in the embryonic heart. *Proc Natl Acad Sci USA* 100(25):15235–15240.

28. Kruse M, et al. (2009) Impaired endocytosis of the ion channel TRPM4 is associated with human progressive familial heart block type I. *J Clin Invest* 119(9):2737–2744.
29. Liu H, et al. (2010) Gain-of-function mutations in TRPM4 cause autosomal dominant isolated cardiac conduction disease. *Circ Cardiovasc Genet* 3(4):374–385.
30. Mathar I, et al. (2010) Increased catecholamine secretion contributes to hypertension in TRPM4-deficient mice. *J Clin Invest* 120(9):3267–3279.
31. Bakker ML, et al. (2012) T-box transcription factor TBX3 reprogrammes mature cardiac myocytes into pacemaker-like cells. *Cardiovasc Res* 94(3):439–449.
32. Wiese C, et al. (2009) Formation of the sinus node head and differentiation of sinus node myocardium are independently regulated by Tbx18 and Tbx3. *Circ Res* 104(3): 388–397.
33. Hoogaars WM, et al. (2007) Tbx3 controls the sinoatrial node gene program and imposes pacemaker function on the atria. *Genes Dev* 21(9):1098–1112.
34. Hoogaars WM, et al. (2004) The transcriptional repressor Tbx3 delineates the developing central conduction system of the heart. *Cardiovasc Res* 62(3):489–499.
35. Frank DU, et al. (2012) Lethal arrhythmias in Tbx3-deficient mice reveal extreme dosage sensitivity of cardiac conduction system function and homeostasis. *Proc Natl Acad Sci USA* 109(3):E154–E163.
36. Kuratomi S, et al. (2009) The cardiac pacemaker-specific channel Hcn4 is a direct transcriptional target of MEF2. *Cardiovasc Res* 83(4):682–687.
37. Naya FJ, et al. (2002) Mitochondrial deficiency and cardiac sudden death in mice lacking the MEF2A transcription factor. *Nat Med* 8(11):1303–1309.
38. Desai BN, et al. (2012) Cleavage of TRPM7 releases the kinase domain from the ion channel and regulates its participation in Fas-induced apoptosis. *Dev Cell* 22(6): 1149–1162.
39. Sah R, et al. (2002) Inhibition of calcineurin and sarcolemmal Ca2+ influx protects cardiac morphology and ventricular function in K(v)4.2N transgenic mice. *Circulation* 105(15):1850–1856.
40. Marger L, et al. (2011) Pacemaker activity and ionic currents in mouse atrioventricular node cells. *Channels (Austin)* 5(3):241–250.
41. Rosen JN, Sogah VM, Ye LY, Mably JD (2013) ccm2-like is required for cardiovascular development as a novel component of the Heg-CCM pathway. *Dev Biol* 376(1):74–85.
42. Neco P, et al. (2012) Paradoxical effect of increased diastolic Ca(2+) release and decreased sinoatrial node activity in a mouse model of catecholaminergic polymorphic ventricular tachycardia. *Circulation* 126(4):392–401.

Supporting Information

Sah et al. 10.1073/pnas.1311865110

SI Methods

Cardiac-Targeted *Trpm7* Knockout Mice. All animal procedures have been reviewed and approved by the Institutional Animal Care and Use Committee at Children's Hospital Boston. Animals were housed under standard conditions and allowed access to food and water ad libitum. Cardiac-targeted knockout mice were generated by crossing $Trpm7^{fl/fl}$ and $Trpm7^{fl/-}$ mice described previously (1) with αMHC-*Cre* (provided by Michael Schneider, Imperial College London, London, England) or *Hcn4-Cre-ERT2* (2) (provided by Andreas Ludwig, Institut fur Experimentelle Klinische Pharmakologie und Toxikologie, Erlangen, Germany) mice. Mice were maintained on 129/SvEvTac mixed genetic background. In the case of *Hcn4-Cre-ERT2* mice, *Cre* recombination was achieved by administering tamoxifen (Tm) at 40 mg/kg by gavage for 4 d. *Cre* recombinase expression and function was assessed by crossing the above cardiac *Cre* lines with $ROSA26^{nTmG}$ reporter mice (3) and imaging isolated cardiomyocytes using an FV1000 confocal microscope (Olympus). Mice were genotyped from tail tip DNA using the following: αMHC-Cre-specific primers (αMHC-Cre-F: 5′-ATG ACA GAC AGA TCC CTC CTA TCT CC-3′; αMHC-Cre-R: 5′-CTC ATC ACT CGT TGC ATC ATC GAC-3′), Hcn4-ERT2-Cre specific primers (Hcn4-CreERT2-F: 5′-GCG AAG GAC GCG TCC TCA CTG GC-3′; Hcn4-CreERT2-R: 5′-ACC GAC GAT GAA GCA TGT TTA GCT GG-3′), and primers flanking exon 17 of *Trpm7* (1) (M7-exon17-F: 5′-GCC ATC TCT CCT CTG GTT TT-3′; M7-exon17-R: 5′-GAT AGA CTA TAT ACT AGG TAC ATG G-3′). Transnetyx Inc performed some of the genotyping. To assess for deletion of *Trpm7* at the level of genomic DNA, DNA was isolated using Purelink Genomic DNA Mini kit (Invitrogen) and PCR performed using primers flanking exon 17 (above).

Embryonic Cardiomyocyte Isolation, Culture, and Adenoviral Transduction. $Trpm7^{fl/fl}$ embryonic hearts (6–11) were removed from embryonic day 13.5–14.0 embryos obtained from pregnant $Trpm7^{fl/fl}$ female mice mated with a $Trpm7^{fl/fl}$ male. The ventricles were cut into <1-mm pieces in PBS and washed with fresh PBS to remove blood. The embryonic heart pieces were then digested for 30 min at 37 °C in 1 mL Hepes-buffered saline solution [HBSS: PBS, 10 mM Hepes, 20% (vol/vol) FBS] with 10 mg of Collagenase A (Roche, catalog no. 11088785103) and 10 mg Collagenase B (Roche, catalog no. 11088823103), vortexing gently every 10 min. The digested heart pieces were then triturated with a 1-mL pipette tip and 10 mL of HBSS added to inactivate the enzyme. The freed embryonic ventricular cardiomyocytes (EVM) were then spun down at 700 rpm for 5 min. The supernatant was discarded and the cell pellet was resuspended in 1–2 mL of differentiation media [DM: Iscove's modified Dulbecco's medium with added: 1% (wt/vol) L-glutamine, 2% (vol/vol) Pen/Strep, 15% (vol/vol)] FBS, 1% (wt/vol) ascorbic acid, and 0.001% monothioglycerol). Cells were then preplated in 1–2 × 35-mm culture dishes for ∼45 min to remove fibroblasts. Media enriched in EVM was then removed and plated on either 35-mm culture dishes or fibronectin-coated 10-mm glass coverslips or 10-mm glass coverslip culture dishes (In Vitro Scientific) for further experiments. Adenoviruses, *Ad-CMV-Lacz*, *Ad-CMV-Cre*, and *Ad-TnT-Cre*, were kind gifts from William Pu, Boston Children's Hospital, Boston, MA. EVM were incubated DM with adenovirus (multiplicity of infection, 100) for 24 h and then washed twice with DM. Experiments were performed 2–5 d after viral transduction.

Ventricular Cardiomyocyte Isolation. Hearts were excised from Avertin-anesthetized, heparin-anticoagulated mice and aortas cannulated with an 18-gauge needle connected to a peristaltic pump. Hearts were then retrograde perfused for 8–10 min at a perfusion pressure of 70–100 mm Hg with either a solution of 0.066 mg/mL Liberase Blendzyme (Roche Diagnostics) or a mixture of 0.4 mg/mL Collagenase B (Roche), 0.3 mg/mL Collagenase D (Roche), and 0.025–0.05 mg/mL Protease XVI (Sigma), in nominally Ca^{2+}-free Tyrode's solution (in mM: 140 NaCl, 5.4 KCl, 10 Hepes, 10 glucose, 1 $MgCl_2$; pH 7.4 with NaOH) warmed to 36 °C. After digestion, hearts were perfused with high [K^+] solution (KB, in mM: 120 K^+ glutamate, 20 KCl, 10 Hepes, 1 $MgCl_2$, 0.3 EGTA, and 10 Glucose; pH 7.4 with KOH), minced with scissors, suspended in KB solution by gentle pipetting, and filtered with a >100-μm mesh cell strainer. Freshly dissociated cardiomyocytes were then used for electrophysiological studies within 6–8 h.

Isolation of Sinoatrial Node Myocytes. Sinoatrial node (SAN) myocytes were isolated as described by Marger et al. (4). Briefly, hearts were removed under general anesthesia, consisting of 10 mg/kg of xylazine (Rompun 2%; Bayer AG) and 100 mg/kg of ketamine or using Avertin anesthesia. The SAN regions were excised in prewarmed (35 °C) Tyrode's solution containing (in mM/L): 140 NaCl, 5.4 KCl, 1.8 $CaCl_2$, 1 $MgCl_2$, 5 Hepes-NaOH, and 5.5 D-glucose; adjusted to pH 7.4 with NaOH. SAN tissue strips were then be transferred into a "low-Ca^{2+}-low-Mg^{2+}" solution containing (in mM/L): 140 NaCl, 5.4 KCl, 0.5 $MgCl_2$, 0.2 $CaCl_2$, 1.2 KH2PO4, 50 taurine, 5.5 D-glucose, 1 mg/mL BSA, and 5 HEPES-NaOH; adjusted to pH 6.9 with NaOH. Tissue was digested by Liberase TH (229 U/mL; Roche), elastase (1.9 U/mL; Boehringer Mannheim), and 200 μM $CaCl_2$. Digestion was carried out for 9–13 min at 35 °C, under manual mechanical agitation. Tissue strips were then washed and transferred into a modified "Kraftbrühe" (KB) medium containing (in mM/L): 70 L-glutamic acid, 20 KCl, 80 KOH, 10 (±)D-β-OH-butyric acid, 10 KH_2PO_4, 10 taurine, 1 mg/mL BSA, and 10 Hepes-KOH; adjusted to pH 7.4 with KOH. Single SAN and AVN myocytes were then isolated by agitation in KB solution at 35 °C. Cellular automaticity was restored by readapting the cells to a physiological extracellular Ca^{2+}concentration by addition of a solution containing (in mM/L): 10 NaCl, 1.8 $CaCl_2$, and normal Tyrode's solution containing BSA (1 mg/mL). The final cell storage solution contained (in mM/L): 100 NaCl, 35 KCl, 1.3 $CaCl_2$, 0.7 $MgCl_2$, 14 L-glutamic acid, 2 (±)D-β-OH-butyric acid, 2 KH_2PO_4, 2 taurine, 1 mg/mL BSA (pH 7.4), and gentamycin (50 μg/mL).

Zebrafish Morpholino. Morpholino targeting the translation start site of zebrafish *trpm7*, designed by Gene Tools, LLC, was diluted to a final concentration of 500 μM in water containing 0.1% phenol red. Wild-type Tubingen strain embryos were injected at the one-cell stage with 0.5 nL morpholino or the same volume of water containing 0.1% (vol/vol) phenol red as a negative control, using a PLI-100 pico-injector (Harvard Instruments) and subsequently raised at 28.5 °C. Morpholino sequence was ATCCAGGACTTCTGGGACATTCT. Heart rates were determined at 20–21 °C at 48 h by counting contractions over 60 s.

Ca^{2+} Imaging of Embryonic Cardiomyocytes. EVMs plated on 10-mm glass-bottom coverslip culture dishes were loaded with 5–10 μM Fluo-4 for 30 min at 37 °C in DM (see above). The cells

were washed twice with DM and then placed on the stage of an FV1000 confocal microscope (Olympus), enclosed in a temperature- and CO_2-controlled chamber set at 37 °C, and maintained at 5% CO_2. Ca^{2+} transients were measured from groups of synchronously contracting EVM in line scan mode (~2- to 4-ms scans) using an Olympus 20× air (N.A. 0.9) objective.

Ca^{2+} Imaging of SAN Myocytes. Spontaneous $[Ca^{2+}]_i$ transients were recorded in both enzymatically isolated primary SAN cells and in individual cells of intact SAN tissue loaded with Fluo-4AM under control (Tyrode's) or isoproterenol at 36 °C. In experiments carried with SAN intact tissue, movement artifacts were avoided by adding 25 μM cytochalasin-D. To detect Ca^{2+} signals, the SAN intact preparation was loaded with the Ca^{2+} indicator Fluo-4AM (20 μM) for 60 min. SAN myocytes were distinguished from other excitable cell types (i.e., atrial cells) by their morphology (spindle and elongated shape) and size (~10 μm diameter). To ensure that recordings obtained in intact SAN tissue came from the dominant pacemaker region, we focused on the central nodal area described by Verhejick et al. (5). Images were obtained with confocal microscopy (Zeiss LSM 780) by scanning the cell with an argon laser in line scan configuration (1.54-ms line rate); fluorescence was excited at 488 nm, and emissions were collected at >505 nm. A 63× water immersion objective (N.A. 1.2) and a 63× oil immersion objective were used to record $[Ca^{2+}]_i$ in isolated SAN cells, wheres a 40× objective (N.A. 1.2) was used for intact SAN tissue. Image analyses were performed by ImageJ software. Images were corrected for the background fluorescence and the fluorescence values (F) were normalized by the basal fluorescence (F_0) to obtain the fluorescence ratio (F/F_0). Integrals of light intensity were analyzed by pClamp software (ver. 9, Axon Instruments Inc.), and $[Ca^{2+}]_i$ transient parameters were analyzed as described previously (6). $[Ca^{2+}]_i$ transient duration was measured from the peak of the $[Ca^{2+}]_i$ transient to 90% decay.

Electrocardiography. ECGs were performed in supine mice sedated using Avertin anesthesia. Dissection pins were placed s.c. in the right arm and left leg. The ECG signal was amplified using a speaker amplifier/mixer and then digitized using a Digidata 1320 board (Molecular Devices) acquired with Clampex (pClamp9; Molecular Devices) and analyzed with Clampfit (Molecular Devices) and Origin software (OriginLab Corporation).

Mouse Telemetry. For telemetric ECG recording, adult male mice were anesthetized with 2% isofluorane. A midline incision was made on the back along the spine to insert a telemetric transmitter (TA10EA-F20; Data Sciences International) into a s.c. pocket with paired wire electrodes placed over the thorax (chest bipolar ECG lead). Local anesthesia was obtained with lidocaine (1%) injected s.c. at the sites of electrodes and transmitter implantation. To manage possible postsurgery pain, Advil (paracetamol and ibuprofen, 7 mL/L) was added to the drinking water for 4 d after implantation. Experiments were initiated at least 8 d after recovery from surgical implantation. Mice were housed in individual cages with ad libitum access to food and water and were exposed to standard 12-h light/dark cycles in a thermostatically controlled room. ECG signals were recorded using a telemetry receiver and an analog-to-digital conversion data acquisition system for display and analysis by Dataquest A.R.T. software (Data Sciences International). Heart rates were determined from interbeat (RR) intervals of the ECG. Mean heart rate values were obtained in each mouse for an overall 24-h period from 8:30 AM to 8:30 PM. AVB and SP were counted in 1-min-long stretches of recordings each hour for 24 h and averaged.

Cellular Electrophysiology. *TRPM7* current was measured in isolated cardiomyocytes in the whole-cell configuration as previously described (1). Extracellular solution composition was (in mM): 135 NaCl, 5.4 CsCl, 10 Hepes, 10 glucose, 0.1 $CdCl_2$, and 1 $CaCl_2$; pH 4.0–7.4 with NaOH. To measure Mg^{2+}-inhibited current, 10 mM $MgCl_2$ was added to the solution and perfused onto cells. Pipette solutions contained (in mM): 120 L-aspartic acid, 20 CsCl, 2.5 EGTA or 1,2-bis(o-aminophenoxy)ethane-N,N,N′,N′-tetraacetic acid, 2.5 EDTA, 10 Hepes, 120 CsOH, 5 Na_2ATP, and 0.5 Na_2GTP; pH 7.2 in CsOH. The voltage protocol (shown in figure insets) held the myocytes at 0 mV, stepped to + 100 mV for 40 ms and then ramped to −80 mV over 500 ms, holding at −80 mV for 40 ms before stepping back to 0 mV. This protocol was repeated every 4–6 s, and recordings continued for 10–15 min per cell until a steady-state *TRPM7* current was obtained. After establishing the whole-cell configuration, cell capacitance transients were recorded by applying 40-ms voltage steps from 0 mV to 10 mV, and cell capacitance was calculated offline.

For measuring the I_f current in SAN cells, the extracellular solution was standard Tyrode's solution with 2 mM $BaCl_2$ added to block I_{K1} (in mM): 140 NaCl, 4 KCl, 10 Hepes, 10 glucose, 1.2 $CaCl_2$; pH 4.0–7.4 with NaOH. The pipette solution contained (in mM): 135 KCl, 1 $MgCl_2$, 0.1 $CaCl_2$, 10 EGTA, 10 Hepes, 5 MgATP, 0.3 NaGTP, and 6.6 phosphocreatine; pH 7.2 with KOH. I_f was defined as the time-dependent, sustained current component at the end of the hyperpolarizing pulse minus instantaneous current.

For measuring I_{CaL} and I_{CaT} in SAN cells we used an intracellular solution containing (in mM): 120 L-aspartic acid, 20 CsCl, 5 EGTA, 10 Hepes, 1 $MgCl_2$, 120 CsOH, 2.5 Mg_2ATP, and 0.1 Na_2GTP; pH 7.2 in CsOH. The extracellular solution contained (in mM): 140 CsCl, 10 Hepes, 10 glucose, 2 $CaCl_2$, 1 $MgCl_2$; pH to 7.4 with CsOH.

Cellular automaticity was recorded under perforated-patch conditions using β-escin to allow proper voltage- and current-clamp conditions and preservation of the intracellular environment. Recordings were performed in extracellular Tyrode's solution (at 36 °C) containing (in mM): 140 NaCl, 5.4 KCl, 1.8 $CaCl_2$, 1 $MgCl_2$, 5 Hepes-NaOH, 5.5 and D-glucose; adjusted to pH 7.4 with NaOH. The composition of the pipette solution allowed recording of K^+-dependent ionic currents and contained (in mM): 130 KCl, 10 NaCl, 2 ATP-Na^+ salt, 6.6 creatine phosphate, 0.1 GTP-Mg^{2+}, 0.04 $CaCl_2$ (pCa = 7), and 10 Hepes-KOH; adjusted to pH 7.2 with KOH. All voltage values were corrected for the appropriate liquid junction potential. Action potential (AP) durations were measured from the peak of the AP to 90% repolarization.

All currents were recorded using an Axopatch 200B amplifier (Molecular Devices), acquired with Clampex (pClamp9; Molecular Devices), and analyzed with Origin software (OriginLab Corporation). Signals were sampled at 10 kHz and low-pass filtered at 5 kHz. Statistical analysis used the two-sample independent Student *t* test.

Quantitative RT-PCR Expression Analysis. mRNA was quantified by quantitative RT-PCR (qRT-PCR) from total RNA isolated from pooled SAN (4–6 SAN/sample) dissected from *KO* or *WT* hearts, or from 35-mm dishes of beating cultured embryonic ventricular myocytes . Random hexamer primed cDNA synthesis was performed using the SuperScript III First Strand Synthesis System for RT-PCR (Invitrogen) using 2–4 μg total RNA. Primers were synthesized by Integrated DNA Technologies, validated by standard PCR, and quality controlled by melting curve analysis after qRT-PCR reactions. Real-time PCR reactions were run in triplicate using the SYBR Green method (ROX as passive reference dye; Affymetrix) in an Eppendorf Mastercycler epgradient S Realplex4 qRT-PCR cycler (Eppendorf) for 40 cycles, and data were analyzed in Microsoft Excel. Quantification was normalized to GAPDH expression.

The primers sequences for the qRT-PCR reactions are as follows:

Gene	Forward primer, 5′–3′	Reverse primer, 5′–3′
GAPDH	TGCACCACCAACTGCTTAG	GATGCAGGGATGATGTTC
Hcn4	GTGGGGGCCACCTGCTATGC	CTGTCGGGTGTCAGGCGGGA
Hcn2	TGTCGGATGGCTCCTATTTC	GCACCTCGTTGAAATTGTCC
Trpm4	CCGCTTCCGCCTTCGGTTTGA	GGGAGCTGAGCTTGGGTGGC
$Ca_v3.1$	ATCTTTGGCATCGTTGGTGT	AGGCTGAGAGCAGATGAAGG
$Ca_v1.3$	CAAGGACTGGTGGGGAAGTA	TTTGGAGTCTTCTGGCTCGT
Serca2a	CCATCTGCTTGTCCATGTCACT	CCAATGGTTTAGGAAGCGGTTACT
Trpm7	GTTGAATTACTGGAACAGTCCTTCAG	CCGTTCCATCCACATATCAGATAACA

1. Jin J, et al. (2008) Deletion of Trpm7 disrupts embryonic development and thymopoiesis without altering Mg2+ homeostasis. *Science* 322(5902):756–760.
2. Herrmann S, Fabritz L, Layh B, Kirchhof P, Ludwig A (2011) Insights into sick sinus syndrome from an inducible mouse model. *Cardiovasc Res* 90(1):38–48.
3. Muzumdar MD, Tasic B, Miyamichi K, Li L, Luo L (2007) A global double-fluorescent Cre reporter mouse. *Genesis* 45(9):593–605.
4. Marger L, et al. (2011) Pacemaker activity and ionic currents in mouse atrioventricular node cells. *Channels (Austin)* 5(3):241–250.
5. Verheijck EE, et al. (2001) Electrophysiological features of the mouse sinoatrial node in relation to connexin distribution. *Cardiovasc Res* 52(1):40–50.
6. Picht E, Zima AV, Blatter LA, Bers DM (2007) SparkMaster: Automated calcium spark analysis with ImageJ. *Am J Physiol Cell Physiol* 293(3):C1073–C1081.

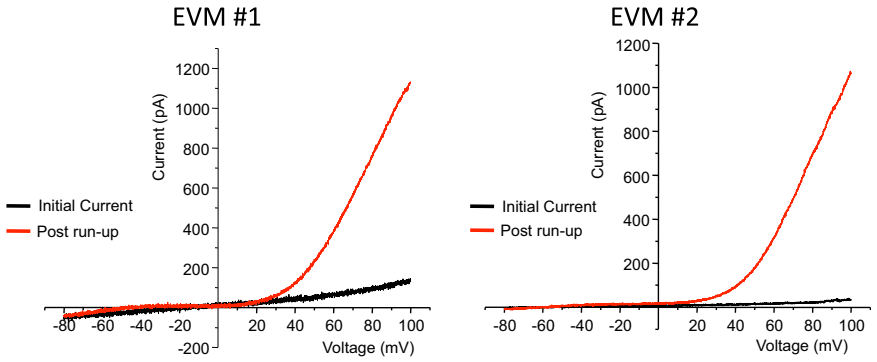

Fig. S1. Activation of native TRPM7 current in cultured EVMs. Representative examples of whole-cell recordings from cultured EVMs (EVM #1 and EVM #2) demonstrating the current on "break-in" (Initial Current) and after 7–10 min of cell dialysis (Post run-up). Note that TRPM7 current is nearly absent on break-in.

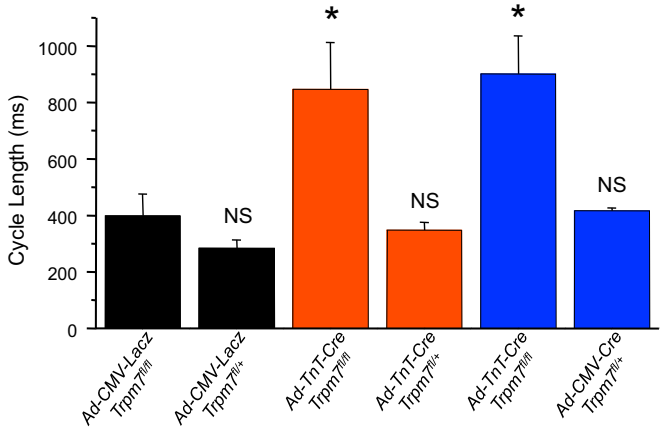

Fig. S2. Ca^{2+} transient cycle lengths in *Trpm7$^{fl/fl}$* and *Trpm7$^{fl/+}$* EVMs. Ca^{2+} transient cycle lengths measured by confocal microscopy using Fluo-4AM in EVM transduced with *Ad-CMV-Lacz-Trpm7$^{fl/fl}$* (n = 18), *Ad-CMV-Lacz-Trpm7$^{fl/+}$* (n = 6), *Ad-TnT-Cre-Trpm7$^{fl/fl}$* (n = 13), with *Ad-TnT-Cre-Trpm7$^{fl/+}$* (n = 12), *Ad-CMV-Cre-Trpm7$^{fl/fl}$* (n = 18), and *Ad-CMV-Lacz-Trpm7$^{fl/+}$* (n = 10). *$P < 0.05$ compared with *Ad-CMV-Lacz-Trpm7$^{fl/fl}$*. NS, not statistically different compared with *Ad-CMV-Lacz-Trpm7$^{fl/fl}$*.

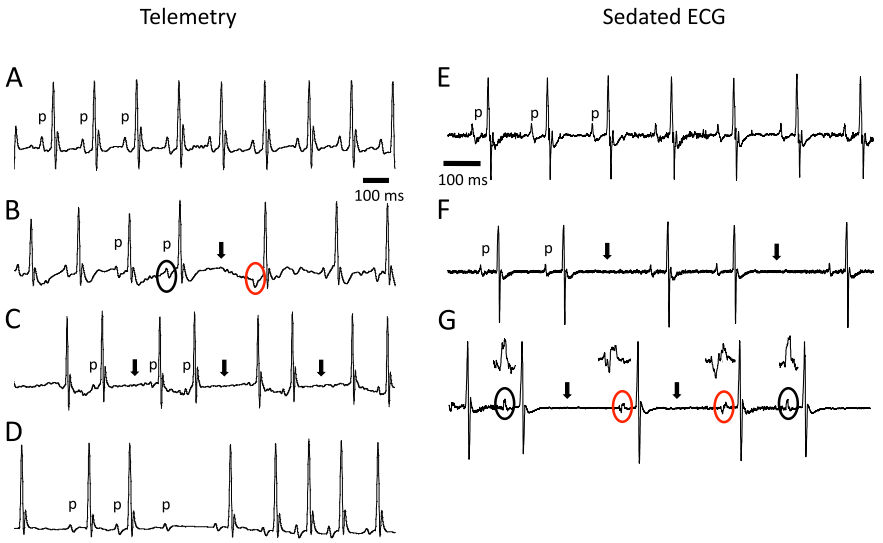

Fig. S3. ECGs by telemetry and in sedated mice. Representative ECGs obtained in conscious mice by telemetry (*A–D*, *Left*) and in sedated mice (*E–G*, *Right*) from *WT* and $KO^{\alpha MHC\text{-}Cre}$ mice. *WT* ECGs show normal sinus rhythm (p indicate p waves) by telemetry (*A*) and with sedation (*E*). Sinus pauses are evident in $KO^{\alpha MHC\text{-}Cre}$ mice by both telemetry (*B*) and sedated ECG (*F*). Solid arrows indicate location of the sinus pause and expected p wave. (*C*) Episode of atrial bigeminy with sinus pause and (*D*) atrioventricular block in telemetered $KO^{\alpha MHC\text{-}Cre}$ mouse. (*G*) Sinus pauses with ectopic atrial foci. Note the change in p wave morphology indicative of change in atrial focus after the sinus pause (red circles, *Inset*) compared with normal p wave (black circle, *Inset*).

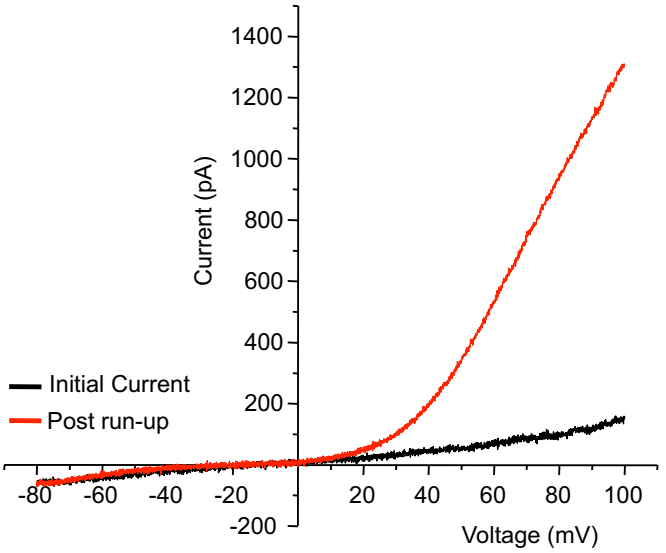

Fig. S4. Activation of native TRPM7 current in freshly isolated SAN cell. Representative example of whole-cell recordings from a freshly isolated SAN cell demonstrating the current on "break-in" (Initial Current) and after 7–10 min of cell dialysis (Post run-up). Note that TRPM7 current is nearly absent on break-in.

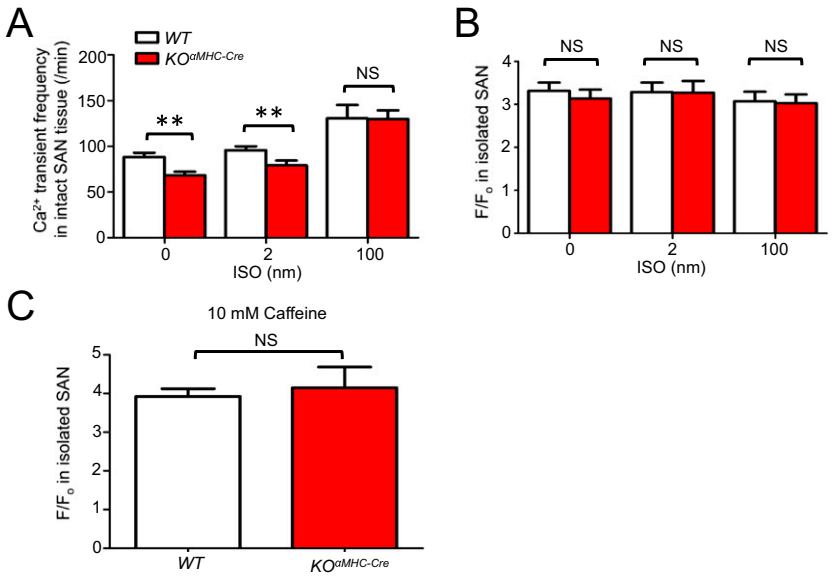

Fig. S5. Ca^{2+} transient characteristics in isolated SAN and in SAN within intact sinoatrial node tissue from *WT* and $KO^{\alpha MHC\text{-}Cre}$ mice. (*A*) Ca^{2+} transient frequency firing frequency of SAN cells within the intact sinoatrial node tissue in *WT* compared with $KO^{\alpha MHC\text{-}Cre}$. (*B*) Peak Ca^{2+} transients are unchanged in isolated *WT* and $KO^{\alpha MHC\text{-}Cre}$ SAN. (*C*) Peak Ca^{2+} transient (F/F_o) in response to application of 10 mM caffeine to isolated SAN cells. $^{**}P < 0.01$. NS, not statistically different.

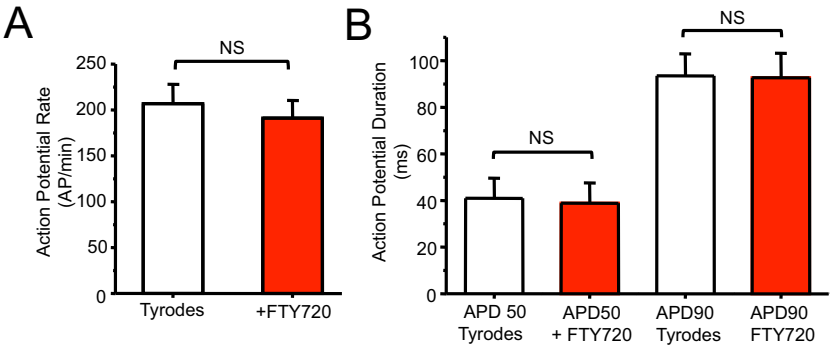

Fig. S6. AP rate and duration of isolated WT SAN in the absence and presence of 500 nM FTY720. (*A*) AP firing rate. (*B*) AP duration at 50% repolarization (APD50) and 90% repolarization (APD90). NS, not statistically different.

Table S1. Action potential characteristics of *WT* and *KO*$^{\alpha MHC\text{-}Cre}$ sinoatrial node cells

	Tyrode's		ISO 2nM		ISO 100nM							
WT/*KO*$^{\alpha MHC\text{-}Cre}$	A	*n*	B	*n*	C	*n*	*P*, A vs. B	*P*, A vs. C	*P*, B vs. C	*P*, *WT* vs. *KO*		
WT												
Rate (bpm)	127 ± 25	7	169 ± 22	7	226 ± 20	7	NS	**	NS	*A	** B	NS C
MDP (mV)	−65 ± 2	7	−68 ± 2	7	−72 ± 1	7	NS	**	NS	**A	* B	*C
Eth (mV)	−43 ± 2	7	−43 ± 2	7	−48 ± 3	7	NS	NS	NS	NS A	NS B	*C
DDSL (mV/ms)	0.09 ± 0.01	7	0.10 ± 0.01	7	0.12 ± 0.03	7	NS	NS	NS	*A	*B	NS C
APA (mV)	79 ± 4	7	88 ± 5	7	98 ± 7	7	NS	NS	NS	NS A	NS B	NS C
dV/dt (mV/ms)	15 ± 6	7	33 ± 9	7	33 ± 10	7	NS	NS	NS	NS A	NS B	NS C
APD (90% repol, ms)	103 ± 15	7	99 ± 11	7	96 ± 8	7	NS	NS	NS	*A	NS B	NS C
KO$^{\alpha MHC\text{-}Cre}$												
Rate (bpm)	39 ± 16	5	53 ± 15	5	161 ± 38	5	NS	**	*			
MDP (mV)	−57 ± 2	5	−61 ± 2	5	−65 ± 2	5	NS	*	NS			
Eth (mV)	−37 ± 2	5	−39 ± 2	5	−39 ± 2	5	NS	NS	NS			
DDSL (mV/ms)	0.03 ± 0.01	5	0.04 ± 0.01	5	0.11 ± 0.03	5	NS	*	*			
APA (mV)	76 ± 7	5	90 ± 7	5	96 ± 6	5	NS	NS	NS			
dV/dt (mV/ms)	12 ± 5	5	26 ± 14	5	29 ± 12	5	NS	NS	NS			
APD (90% repol, ms)	172 ± 23	5	156 ± 19	5	110 ± 7	5	NS	*	*			

APA, action potential amplitude; APD, action potential duration at 90% repolarization; DDSL, diastolic depolarizeation slope; dV/dt, action potential upstroke velocity; Eth, action potential threshold; MDP, mean diastolic membrane potential; NS, not statistically different; Rate, action potential firing rate. *$P < 0.05$; **$P < 0.01$.